IEEE Access
Multidisciplinary | Rapid Review | Open Access Journal

Received 27 February 2023, accepted 21 March 2023, date of publication 29 March 2023, date of current version 4 April 2023.

Digital Object Identifier 10.1109/ACCESS.2023.3262931

RESEARCH ARTICLE

Fairness-Aware Resource Allocation in Multi-Source WPCN in the Finite Blocklength Regime

NING GUO[1,2], (Student Member, IEEE), XIAOPENG YUAN[1,2], (Graduate Student Member, IEEE), YULIN HU[1,2], (Senior Member, IEEE), AND ANKE SCHMEINK[2], (Senior Member, IEEE)

[1]School of Electronic Information, Wuhan University, Wuhan, Hubei 430072, China
[2]Chair of Information Theory and Data Analytics, RWTH Aachen University, 52074 Aachen, Germany

Corresponding authors: Xiaopeng Yuan (yuan@inda.rwth-aachen.de) and Yulin Hu (hu@inda.rwth-aachen.de)

This work was supported in part by the China National Key Research and Development Program under Grant 2021YFB2900301, in part by the Hubei Key "Jiebang" Research Program under Grant 2021BEC023, in part by the German Research Council (DFG) through the Basic Research Project under Grant DFG SCHM 2643/17, and in part by the Federal Ministry of Education and Research of Germany in the Program of "Souverän. Digital. Vernetzt." Joint Project 6G-Research and Innovation Cluster (RIC) under Grant 16KISK028.

ABSTRACT In this work, we investigate a wireless powered communication network (WPCN) where multiple sources are jointly utilized for wireless power transfer (WPT). By consuming the energy harvested from the these WPT sources, a set of sensors are expected to accomplish reliable transmissions carried by finite blocklength (FBL) codes. This work proposes a fairness-aware resource allocation design with low-complexity in such a multi-source WPCN, where the practical nonlinear energy harvesting process is considered (including the effects of components nonlinearity in rectifier circuits and mutual interference between multiple radio frequency signals). In particular, a joint power and blocklength optimization problem minimizing the maximum reliability of all short packet transmissions is considered. To cope with the formulated extremely intractable nonconvex problem, we decompose it into two subproblems, i.e., a power allocation problem and a blocklength allocation problem, nevertheless, both of which are still nonconvex. To address the power allocation subproblem, auxiliary variables are introduced. Subsequently variable substitutions are performed to convert the problem into one being analytically tractable, and an efficient iterative approach is provided via applying the successive convex approximation technique. For the blocklength allocation problem, we for the first time verify the convexity of error probability with respect to blocklength under a harvested energy constraint, which is of great theoretical value and can be extended to numerous applications with energy limitations. Finally, by alternatingly addressing the two subproblems, an efficient sub-optimal solution to the original problem is achieved. We provide numerical results to validate and evaluate the proposed design, and a set of guidelines are provided for practical system designs.

INDEX TERMS Finite blocklength regime, wireless power transfer, resource allocation.

I. INTRODUCTION

In future sixth generation (6G) communication systems, extremely massive connectivity is one of the major key performance indicator to enable the so-called Internet of Everything (IoE) [1], [2], in which massive devices are expected to exchange information or work cooperatively [3] in various kinds of sophisticated applications (e.g., industrial automation, intelligent transportation, smart city). Meanwhile, the explosive number of connected devices raises new requirements from two aspects: 1) how to provide stable and low-cost energy supplement to massive devices [4] and 2) how to allocate limited communication resources among massive devices to achieve high-efficient communication [5], [6].

The associate editor coordinating the review of this manuscript and approving it for publication was Francisco Rafael Marques Lima.

In particular, future IoE is expected to pose significant challenges to traditional power supplement methods [7], e.g., batteries and cabling, due to their limitations with respect to lifespan, capacity, costs and so on. In addition, laying out cables recharging the batteries or replacing batteries (by human beings or robots) may lead to significant inconvenience and costs especially in networks with massive devices. Therefore, novel energy-powering approaches are urgently required to match the future IoE requirements. Harvesting energy from the environment (e.g., wind turbines, solar cells) is an easy and eco-friendly solution [8]. Nevertheless, these natural energy sources are unstable and might be inaccessible under numerous applications, e.g., indoors smart home, autonomous control in factories and curves environmental information detection. To cope with it, radio frequency (RF) is a promising and practical energy source [9], [10], which can be utilized as energy carrier. RF based energy harvesting (EH) [10], [11], [12], [13], [14], as a form of a wireless power transfer (WPT) technique, is capable of converting the received RF signals into beneficial electricity resource in a more controllable and stable manner [15], which enables flexible instant charging to satisfy practical service requirements. More importantly, devices can be powered simultaneously from the same RF signal, which facilitates the power supplement in large-scale device networks.

So far, such RF-based WPT technology, verified as a secure and efficient energy-powering approach, has been integrated to wireless networks to support the potentially massive unsourced wireless devices in a variety of scenarios [16], [17], [18], [19]. Nevertheless, computation-intensive and latency-sensitive communication in future 6G is still challenging due to the limited communication resources (e.g., power, time, spectrum, etc). To guarantee energy-efficient communication, resource allocation (including power, time and etc.) has become an important research direction and numerous efforts have been made to improve the performance of wireless power communication networks (WPCN) [20], [21], [22], [23]. Authors in [24] proposed an optimal time and power allocation design for sum α-fair utility maximization in a WPCN. In [25], authors investigated a dynamic-TDMA-based WPCN and obtained the optimal time allocation strategy in a closed-form expression targeting to maximize the throughput. Authors in [26] proposed a multidimensional resource allocation framework based on a heterogeneous mobile architecture to achieve effective implementation of federated learning. To improve the energy efficiency, authors in [27] investigated a time, subcarrier, and power allocation schemes in OFDMA multicell networks. Nevertheless, the aforementioned results are conducted under the assumption of an ideal linear EH process, which is likely inaccurate in practical. Due to the component nonlinearity in rectifier circuits, the output DC power in the EH process has actually a complicated nonlinear relationship with the received RF power [28]. To ensure the effectiveness of resource allocation strategies in realistic system designs, nonlinear impact of the EH process should be considered, especially in WPCN supporting short packets transmissions, where power has significant influence on communication performances in terms of reliability.

Recently, some studies have proposed resource allocation designs while considering the practical nonlinear EH model [29], [30], [31], [32], [33], but only a single WPT is deployed as energy supplier. In practice, the path-loss is usually considerable and the RF-DC conversion efficiency is usually low [34], it is likely difficult to guarantee reliable communications with only a single WPT source. Moreover, upperbounded by the hardware, the transmit RF power from a single source is limited, i.e., the achievable WPT capacity is restricted, which may lead to insufficient power supplement and accordingly result in low effective WPT. To cope with this, introducing more WPT sources has been verified as an effective solution [35]. By combining the multiple RF signals from multi-source, a higher WPT efficiency and a higher energy ceiling can be achieved, which contributes to further system performance enhancement. One the one hand, a higher flexibility is enjoyed by exploiting multiple WPT sources, which is likely to lead to a higher EH (RF-DC) conversion efficiency and thus improving the WPCN performance. On the other hand, the diversity of channels is introduced by multiple sources, and with the assistance of which the negative impacts of deep fading at certain channels can be compensated. In other words, the WPT performance to devices are expected to be improved via enjoying one or more relatively superior links (sources).

Although the joint utilization of multiple WPT sources has the potential to improve the energy efficiency and accordingly enhance the system performance, a great deal of challenges are also introduced for system analysis and the corresponding reasonable resource scheduling schemes are indispensable prerequisites for high-efficiency energy transfer achievement. On the one hand, according to [36], where an analytical EH model for multi-source WPT system is proposed, the mutual interference among multiple received RF signals has a significant effect on the waveform of the received signal at device, which should not be ignored. More importantly, such interference can potentially lead to either positive or negative impacts on the RF-DC conversion efficiency, which will further pose an unpredictable impact on the WPT efficiency of the system. In other words, to avoid these potential negative influences on the WPT process, appropriate resource allocation based on accurate EH model is essential to be inevestigated. On the other hand, when the total available resources (e.g., power) are limited, diverse resource scheduling schemes among sources will result in different system performances (e.g., reliability, delay, throughput). In order to sufficienctly utilize the limited resource and optimally satisfy diverse quality of service (QoS) requirements in numerous types of networks, appropriate resource allocation schemes are urgently needed accordingly. Authors in [37], formulated a joint energy management and user scheduling problem

in a multi-source energy harvesting wireless networks, but the operations of the WPT process at different sources are not cooperative, i.e., a joint design among them is missing. In work [38], a power allocation design among sources has been proposed, nevertheless, under a fixed frame structure, i.e., the blocklength for WIT are unadjustable and only a single dimension of resource (power) is optimized. In [39], multiple sources are utilized for WPT, but the fairness-aware resource allocation is out of the scope of their work. Note that the sizes of the data packets generated at IoT devices are possibly small and thus that the transmissions of these packets are usually carried via short blocklength codes, e.g., communications operate in the so-called finite blocklength (FBL) regime. In such case, the FBL impacts as well as the impacts of the competitive blocklength allocations among devices on the WPCN performance should be considered in the system designs.

However, to the best of our knowledge, the fairness-aware resource allocation design in a multi-source WPCN are still open issues. We address such issues in this work via investigating a multi-source WPCN supporting FBL communications of different sensors. Activated by the multiple WPT sources, multiple sensors are supposed to realize reliable short packet transmissions. Taking the nonlinear EH impact into account, we study the error probability of the WPCN in the FBL regime and propose a joint power and blocklength allocation design minimizing the modelled error probability.

The main contributions of the work are summarized as follows. First of all, we provide a fairness-aware reliability characterization in multi-source WPCN. In particular, considering the fairness among multiple sensors, we characterize the FBL min-max error probability, which is jointly influenced by the multiple WPT source power and the multiple WIT blocklength. A realistic EH nonlinear model is adopted, which considers the impacts of the mutual interference among multiple RF signals as well as the components nonlinearity in rectifier circuit. Secondly, based on the characterization, we formulate a joint resource allocation problem with the objective of minimizing the maximum error probability of short packet transmissions. To address the formulated nonconvex and extremely intractable problem (due to the nonlinear EH process, complex FBL transmission model and multidimensional optimization variables), we decompose it into two nonconvex but relatively tractable subproblems, i.e., power allocation problem and blocklength allocation problem. By introducing auxiliary variables, performing variable substitutions and successive convex approximation (SCA), the subproblems are respectively reformulated and alternately addressed, through which a suboptimal solution to the original problem can be achieved. Thirdly, for the first time we prove that with a given amount of energy consumption, the transmission error probability of the considered multi-source WPCN network is convex with respect to the short packet transmission blocklength. Such proved convexity may be of interest to latency-sensitive communication network analysis and inspire numerous studies regarding energy limited ultra reliable low latency communications (URLLC) and facilitate the corresponding blocklength allocation designs. Lastly, numerical results have been provided to confirm the analytical model and validate the performance of our proposed algorithm. In particular, the simulation results have validated the illustrated the significant performance enhancements of our proposed joint resource allocation design compared with the benchmarks. In addition, we observe that the increasing of certain resources (e.g., WIT blocklength) has limited ability for further reliability enhancement, which provides guidelines for practical low-cost, high-reliability and low-latency system designs.

The remaining part of this work is organized as follows: Section II describes the system model and review the performance models of FBL transmissions as well as the nonlinear EH with multiple RF sources. In Section III, we characterize the FBL reliability and formulate a joint resource allocation problem. In Section IV, we decompose the intractable original problem into two subproblems and respectively address them. Finally, numerical results are presented and discussed in Section V while the whole work is concluded in Section VI.

II. PRELIMINARIES

A. SYSTEM MODEL

As depicted in Fig. 1, we focus on a multi-source WPCN, where M sources perform WPT to N EH sensors nodes to activate their short packets transmissions to a destination node. All the sources are assumed to have sufficient energy e.g., via wires connection to the power supplier, thus being able to perform the required WPT process. The data amount of the short packet transmitted from sensor i is defined as $k_i, \forall i = 1, \ldots, N$. In particular, each sensor is equipped with an energy harvester, through which the received RF signals at sensor i (received from multiple WPT sources) are converted to DC signals, which can further be utilized for EH. Subsequently, by consuming all the harvested energy, the short packet transmission from sensor i to the destination node is activated. Under such harvest-then-transmit protocol, an operation frame of the network is separated into a WPT phase as well as a WIT phase as shown in Fig. 1.

During the WPT phase, since sufficient energy has been buffered by sources, it is reasonable to assume that all the sources are capable of providing stable power supplement for sensors, i.e., the transmit power of M sources are respectively unchanged during the entire WPT phase. The transmit power of source j is denoted by P_j and the time length for WPT is written as $T_s n_0$, where n_0 denotes the blocklength (length in symbol) of WPT phase and T_s denotes the time length per symbol. The channel gain between source j to sensor i is denoted by $z_{i,j}$. Thus, the received RF power at sensor i from source j can be given as $P_j z_{i,j}$. Once sensor i receives the RF signals from sources, the EH process is activated, in which the received RF signals are converted to DC signals through rectifier circuit in EH unit. Then, for sensor i, DC signals

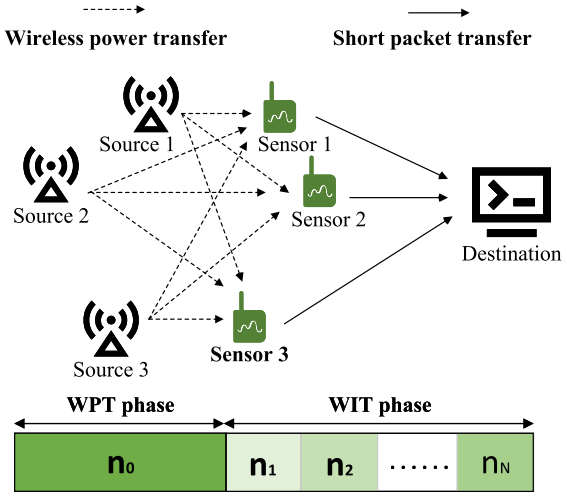

FIGURE 1. System model and the frame structure.

are converted to usable electricity with power of $P_{dc,i}, \forall i = 1, \ldots, N$.

During the WIT phase, N sensors respectively transmit short packets to the destination node by consuming all their harvested energy during the WPT phase, which indicates an energy causality limitation between WPT phase and WIT phase. The entire WIT phase is conducted in a time-division duplex (TDD) manner, i.e., N short packets are sequentially transmitted to the destination, and the co-channel interference can be avoided. We assume the short packet transmissions are required to be completed under low latency and high reliability constraints. For instance, a possible scenario would be in a multi-sensor fusion (MSF) application, where information from multiple sensors are transmitted, synthesized and analyzed automatically by the control terminal under certain guidelines. Based on the analysis results, a set of decisions will be made by the control terminal, e.g., driverless car motion decisions. To guarantee the correctness and timeliness of decision making, all the sensing data require to be transmitted in an URLLC manner, i.e., the sensing data are supposed to be transmitted successfully and all packets transmission should be completed within a preconfigured time limitation. Due to the constraint of latency, transmissions from sensors to the destination node are carried via FBL codes. We denote by n_{total} the maximum available blocklength under the latency constraint, i.e., total amount of symbols permitted during the WIT phase. Accordingly, the time length of the entire WIT phase is limited with $\sum_{i=1}^{N} n_i T_s \leq n_{total} T_s$, where n_i denotes the blocklength (amount of symbols) for short packet transmission from sensor i to the destination node and T_s denotes the duration of a single symbol. In the FBL regime, the decoding errors should be considered. In this work, we consider a reliable transmission scenario, where the transmission error probability of each packet should be at lest lower than 0.1, i.e., $\varepsilon_i \leq 0.1, \forall i = 1, \ldots, N$, where ε_i denotes the error probability of short packet transmission from sensor i to the destination node. Moreover, as the transmission time length of each packet is short, the channels involved are assumed to be block-fading, i.e., the channel is assumed to be constant during one block and varies independently from one transmission to the next. Additionally, we assume that each sensor is equipped with a transceiver capable of transmitting its own channel state information (CSI) to the WPT sources, indicating that the CSI is available at the WPT source nodes. Similarly, the CSI between sensor and destination node is available at each sensor node by classic channel estimation methods. In particular, the channel gain between R_i to D is expressed as $\bar{z}_{2,i}, \forall i = 1, \ldots, N$, and the noise power is denoted by σ^2.

It is worthwhile mentioning that, all sensors have no other energy-powering sources other than the RF energy from the transmitter source and their harvested energy during WPT phase is assumed to be completely consumed for short packet transmission during WIT phase, which indicates that the transmit power of sensor i is jointly influenced by the harvested energy $Q_{ch,i} n_0 T_s$ and its short packet transmission time length $n_i T_s$, i.e., $\bar{P}_i = \frac{Q_{ch,i} n_0 T_s}{n_i T_s}$ holds, where $\bar{P}_i$ denotes the transmit power of sensor i and $Q_{ch,i}$ denotes the harvested power at sensor i. In addition, in our proposed WPCN, the source power and WIT blocklength can be dynamically adjusted. It is critical to note that the realistic RF-DC conversion efficiency is around a lower level, which necessitates the reasonable resources scheduling among multiple sources and multiple sensors to achieve high reliability short packet transmissions under limited resources restrictions.

B. NONLINEAR EH MODEL

During the EH process, the received RF signals at the sensors are first converted to DC signals for electricity reservation. In a recent work [36], a performance characterization is provided for a WPT system with multiple sources sending independent RF signals, where the harvested DC power at a EH receiver is given by

$$P_{dc} \triangleq F_{eh}(\boldsymbol{Q}) \approx \left(\frac{1}{a} W_0(a e^{a I_s} \varphi(\mathbf{Q})) - I_s \right)^2 \hat{R}_L, \quad (1)$$

with $\varphi(\mathbf{Q}) = I_s + \sum_{i=1}^{n_0} \beta_i \sum_{\sum_{m=1}^{M} i_m = i} \hat{\mathcal{C}}_{i,\{i_m\}} \prod_{m=1}^{M} Q_m^{i_m/2}$, where n_0 denotes the truncation order (having influences on the accuracy for modelling the nonlinearity), $\boldsymbol{Q} \triangleq (Q_1, \ldots, Q_M)$ is the set of M received RF signal powers. $\hat{\mathcal{C}}_{i,\{i_m\}} = \frac{M!}{\prod_{m=1}^{M} i_m!} \prod_{m=1}^{M} \lambda_{m,i_m}$ is a constant, and $\beta_i = \bar{k}_i R_{ant}^{\frac{i}{2}}$ is also a constant with $\bar{k}_i = \frac{I_s}{i!(n v_t)^i}$. In addition, $a = \frac{\hat{R}_L}{n v_t}$ is a constant with $\hat{R}_L$, n and v_t being the load resistance, the ideality factor, and the thermal voltage, respectively. Moreover, I_s is the reverse bias saturation current, which is usually not considered in linear EH models. $W_0(\cdot)$ represents the principle branch of Lambert W function, which is the inverse function to $f(x) = xe^x$. Furthermore, R_{ant} represents the matched antenna impedance. It should be pointed out that the mutual interference among the multiple received RF signals cannot be ignored, which is represented by $\prod_{m=1}^{M} Q_m^{i_m/2}$ in

$\varphi(\mathbf{Q})$ and such interference can either positively or negatively influence the WPT efficiency, which makes the considered multi-source WPCN be more challenging than one with only a single WPT source. Clearly, a corresponding appropriate power allocation design among multi-source is of significant importance in high efficiency WPT realization.

C. TRANSMISSIONS IN THE FBL REGIME

Considering the small data amount of packets generated from sensors and the low-latency requirements, short packet are assumed to be transmitted in the FBL regime, in which the transmission error is non-negligible. Based on [41] and [40], the error probability is jointly influenced by the SNR γ, coding rate r and blocklength n, which is given by

$$\varepsilon = \mathcal{P}(\gamma, r, n) \approx Q\left(\sqrt{\frac{n}{\mathcal{V}(\gamma)}}\left(\mathcal{C}(\gamma) - r\right)\right), \tag{2}$$

where $\mathcal{C}(\gamma) = \log(1+\gamma)$ represents the Shannon capacity and $\mathcal{V}(\gamma) = \left(1 - \frac{1}{(1+\gamma)^2}\right)\log_2^2 e$ represents the channel dispersion. $Q^{-1}(\cdot)$ is the reverse of the Gaussian Q-function, which is given by $Q(x) = \int_x^\infty \frac{1}{\sqrt{2\pi}} e^{-t^2/2} dt$.

III. JOINT RESOURCE ALLOCATION PROBLEM FORMULATION

In this section, we first characterize the FBL error probability in the multi-source WPCN and subsequently formulate a joint power and blocklength allocation problem with the objective of minimizing the maximum error probability of short packets transmissions.

A. FBL RELIABILITY CHARACTERIZATION

In the WPT phase, M sources conduct WPT simultaneously in a broadcasting manner and the received power at sensor i from source j is given by

$$Q_{i,j}(P_j) = P_j z_{i,j}, \tag{3}$$

where P_j denotes the power of RF signals transmitted from source j and $z_{i,j}$ denotes the channel gain between source j and sensor i. Subsequently, the multiple RF signals are combined and converted to DC for EH. The harvested power at sensor i is given as

$$P_{dc,i}(\boldsymbol{P}) = F_{eh}\left(\boldsymbol{Q}_i(\boldsymbol{P})\right), \tag{4}$$

where $\boldsymbol{Q}_i$ denotes the set of the multiple received RF power at sensor i, i.e., $\boldsymbol{Q_i} \triangleq (Q_{i,1}, \ldots, Q_{i,j}, \ldots, Q_{i,\mathrm{M}})$ and $F_{eh}(\cdot)$ characterizes the practical nonlinear relationship between the charged power and the received power during EH process. For details, see (1) in II-B. Based on the assumption of stable EH capability of EH units, the harvested power $P_{dc,i}(\boldsymbol{P})$ is considered to be unchanged during WPT phase. Thus, during WPT phase, the total harvested energy at sensor i with duration $n_0 T_s$ is given as

$$E_i(\boldsymbol{P}) = P_{dc,i}(\boldsymbol{P}) n_0 T_s. \tag{5}$$

By consuming the harvested energy, sensors transmit short packets to the destination during the WIT phase. Specifically, the WIT phase is further divided into N slots, and the sensor i transmit the short packet in the i-th slot with duration $n_i T_s$ in timelength. We assume each sensor continuously performs WIT with a stable capacity, i.e., the transmit power of sensor i is unchanged during its frame of short packet transmission, which is jointly affected by the harvested power $P_{dc,i}(\boldsymbol{P})$ and the WIT blocklength n_i:

$$\bar{P}_i(\boldsymbol{P}, n_i) = \frac{E_i(\boldsymbol{P})}{n_i T_s} = \frac{P_{dc,i}(\boldsymbol{P}) n_0}{n_i}, \quad \forall i \in \{1, 2, \ldots, N\}, \tag{6}$$

where n_0 denotes the WPT blocklength, which is a given positive constant. With sensor transmit power $\bar{P}_i$, the signal-to-noise (SNR) of short packet transmission from sensor i to the destination can be written as

$$\gamma_i(\bar{P}_i(\boldsymbol{P}, n_i)) = \frac{\bar{P}_i(\boldsymbol{P}, n_i)\bar{z}_{2,i}}{\sigma_i^2}, \tag{7}$$

where $\bar{z}_{2,i}, \sigma_i^2$ are positive constants. To guarantee reliable short packets transmissions, we set a lower bound limitation for the SNR. We assume that the SNR of all the short packet transmissions should be larger than 1, i.e., $\gamma_i \geq 1, i \in \{1, \ldots, N\}$ must be satisfied. The coding rate of the transmission from sensor i to the destination is given as $r_i(n_i) = \frac{k_i}{n_i}$, where k_i denotes the data amount of the short packet (transmitted from sensor i). Recalling the FBL transmission model (2), with SNR γ_i, coding rate r_i and blocklength n_i, the transmission error probability from sensor i to the destination is represented by

$$\varepsilon_i(\boldsymbol{P}, n_i) = \mathcal{P}\left(\gamma_i(\bar{P}_i(\boldsymbol{P}, n_i)), r_i(n_i), n_i\right). \tag{8}$$

Obvisously, the FBL reliability is jointly affected by the multiple WPT source power and the WIT blocklength. To achieve the desired network performance in supporting a group of sensors' reliable short packets transmission, choosing appropriate transmission power among multiple sources and blocklength among WIT sensors is necessary, especially in a WPCN with URLLC requirement.

B. JOINT RESOURCE ALLOCATION PROBLEM FORMULATION

Considering the fairness among multiple sensors, we aim to minimize the maximum transmission error probability among all sensors by jointly optimizing the multiple source power as well as the multiple WIT blocklength for short packets' transmission. The joint resource allocation

problem is formulated as:

$$(\text{OP}): \min_{\{\boldsymbol{P}\},\{\boldsymbol{n}\}} \max_{i\in\{1,\ldots,N\}} \varepsilon_i(\boldsymbol{P}, n_i) \tag{9a}$$

$$s.t.: \frac{\bar{P}_i(\boldsymbol{P}, n_i)\bar{z}_{2,i}}{\sigma_i^2} \geq 1, \tag{9b}$$

$$\frac{k_i}{n_i} \leq \log_2\left(1 + \frac{\bar{P}_i(\boldsymbol{P}, n_i)\bar{z}_{2,i}}{\sigma_i^2}\right), \tag{9c}$$

$$\sum_{j=1}^{M} P_j \leq P_{total}, \tag{9d}$$

$$0 \leq P_j \leq P_{max}, \tag{9e}$$

$$\sum_{i=1}^{N} n_i \leq n_{total}, \tag{9f}$$

where term $\frac{\bar{P}_i(\boldsymbol{P},n_i)\bar{z}_{2,i}}{\sigma_i^2}$ in (9b) denotes the SNR of short packet transmission from sensor i to the destination, which should be no smaller than 1 to satisfy a basis requirement of reliable transmission. Constraint (9c) specifies the Shannon capacity restriction. Constraint (9d) limits the total available transmit power at multiple sources. Constraint (9e) specifies the maximum transmit power of each source for WPT. Finally, constraint (9f) announces the upper bound of the total blocklength (latency) restriction during WIT phase.

Obviously, the Original Problem (OP) is a nonconvex nonlinear problem and is intractable due to the following reasons. First, during WPT phase, the interference introduced by the multiple received RF signals at sensor i from multiple WPT sources is non-negligible, which combined with the component nonlinearity in the rectifier circuits, make the charged power a complicated nonlinear function with respect to the multiple source power. Such nonlinearity makes the convexity between ε_i and multi-source power $\boldsymbol{P}$ unpredictable and accordingly makes the joint convexity of ε_i with respect to $(\boldsymbol{P}, \boldsymbol{n})$ hardly expected. Second, in the FBL regime, the error probability ε_i is a complex Q-function with respect to SNR $\gamma_i(\boldsymbol{P}, n_i)$, coding rate $r_i(n_i)$ and blocklength n_i, which poses significant difficulty to problem resolution. Third, the error probability is coupled with both two phases (WPT and WIT phase). In particular, error probability ε_i is jointly and directly influenced by (γ_i, r_i, n_i). Moreover, $\boldsymbol{P}$ and n_i have a joint influence on γ_i, and subsequently on the error probability ε_i, which has introduced analysis difficulty in addressing the Original Problem (OP).

IV. PROBLEM REFORMULATION AND SOLVING

A. ORIGINAL PROBLEM DECOMPOSITION

To address such a complicated nonconvex joint resource allocation problem with complex coupling relationships, block coordinate descent (BCD) based problem decomposition is an effective solution. Decomposition, as a divide and conquer strategy, is capable of breaking the hard problems into multiple relatively simpler and mutual independent subproblems, which significantly increases the solvability of the problem. BCD regime, as a simple iterative algorithm for nonconvex optimization, sequentially minimizes the objective function in each block coordinate while holding the other coordinates fixed. In particular, we decompose the Original Problem (OP) into two subproblems, i.e., power allocation problem and blocklength allocation problem, in both of which, only a singular domain of resource (power or blocklength) requires to be optimized, thus the mutual influence between power and blocklength can be decoupled in optimization. Subsequently, a near-optimal solution can be obtained by sequentially addressing the power allocation and blocklength allocation problem until the result converges. The decomposed power allocation problem and blocklength allocation problem are respectively defined as follows.

Definition 1 (Power Allocation Problem): Power allocation problem refers to the process of deciding the amount of transmit power allocated to each WPT source with a given WIT blocklength scheduling scheme. In particular, the transmit power from source j is denoted by $P_j, \forall j = 1, \ldots, M$, which are variables that have to be optimized. Considering the limited WPT capacity of a single WPT source, P_j is upper-bounded by P_{max}, which is a fixed value and $P_j \leq P_{max}$ must be satisfied. The total available transmit power of M sources is denoted by P_{total}, which is a positive constant. Thus, we have $\sum_{j=1}^{M} P_j \leq P_{total}$. Based on the definition, the power allocation problem (SP1) is formulated as:

$$(\text{SP1}): \min_{\{\boldsymbol{P}\}} \max_{i\in\{1,\ldots,N\}} \varepsilon_i(\boldsymbol{P}) \tag{10a}$$

$$s.t.: \frac{\bar{P}_i(\boldsymbol{P})\bar{z}_{2,i}}{\sigma_i^2} \geq 1, \tag{10b}$$

$$\frac{k_i}{n_i} - \log_2\left(1 + \frac{\bar{P}_i(\boldsymbol{P})\bar{z}_{2,i}}{\sigma_i^2}\right) \leq 0,$$
$$(9d), (9e). \tag{10c}$$

Definition 2 (Blocklength Allocation Problem): Blocklength allocation problem refers to the process of deciding the amount of symbols to each sensor for short packet transmission under given multiple source power setups. With fixed symbol duration T_s, blocklength allocation is indeed a time allocation among sensors. Under low-latency restriction, the total available blocklength of N sensors is denoted by n_{total} and $\sum_{i=1}^{N} n_i \leq n_{total}$ must be satisfied. The blocklength allocation problem is given as:

$$(\text{SP2}): \min_{\{\mathbf{n}\}} \max_{i\in\{1,\ldots,N\}} \varepsilon_i(n_i) \tag{11a}$$

$$s.t.: \frac{\zeta_i}{n_i} \geq 1, \tag{11b}$$

$$\frac{k_i}{n_i} \leq \log_2\left(1 + \frac{\zeta_i}{n_i}\right) \tag{11c}$$

$$\sum_{i=1}^{N} n_i \leq n_{total}. \tag{11d}$$

where ζ_i in constraint (11b) is defined as $\zeta_i = \frac{\bar{P}_i(\boldsymbol{P})n_0\bar{z}_{2,i}}{\sigma^2}$, which is a positive constant with given multiple source power $\boldsymbol{P}$.

Clearly, based on the aforementioned problem decomposition, the original extremely complicated problem has been converted to two subproblems, which significantly facilitates the problem settlement. For one thing, the joint effect of power and blocklength on error probability has been decoupled via decomposition, which facilitates the investigation of the convexity of FBL reliability respectively with respect to the power and blocklength and accordingly assists to address the subproblems. For another thing, under such decomposition, power and blocklength are independently optimized without mutual influence, which introduces more flexibility when scenarios changes (e.g., under fixed frame structure, blocklength is non-adjustable) and enables higher extensibility to a variety of power or blocklength optimization scenarios. In the following subsections, we respectively provide solutions to the Subproblem (SP1) and Subproblem (SP2).

B. SOLUTION TO SUBPROBLEM (SP1)

In this subsection, we introduce auxiliary variables and utilize SCA algorithm to reformulate the Subproblem (SP1) and obtain a corresponding suboptimal solution via iteration based method.

In Subproblem (SP1), with given blocklength n_0 and $\boldsymbol{n}$, the transmit power of sensor i is completely influenced by multiple source power $\boldsymbol{P}$, which is given as

$$\bar{P}_i(\boldsymbol{P}) = \frac{E_i(\boldsymbol{P})}{n_i T_s} = \frac{n_0}{n_i} P_{dc,i}(\boldsymbol{P}), \quad \forall i \in \{1, 2, \ldots, N\}. \tag{12}$$

Nevertheless, Subproblem (SP1) is non-convex and cannot be solved by convex optimization tools. First, due to the nonlinear EH process during WPT phase, the SNR (γ_i) of the short packet transmission from sensor i is a complicated nonlinear function with respect to the transmit power of multi-source ($\boldsymbol{P}$), which combined with the complex FBL transmission model (2), makes the object function not necessary convex, i.e., the convexity of ε_i with respect to $\boldsymbol{P}$ unpredictable. Second, constraints (10b) and (10c) are not necessary convex since the concavity of terms $\frac{\bar{P}_i(\boldsymbol{P})\bar{z}_{2,i}}{\sigma_i^2}$ and the convexity of term $-\log_2\left(1 + \frac{\bar{P}_i(\boldsymbol{P})\bar{z}_{2,i}}{\sigma_i^2}\right)$ are not strictly guaranteed. As a consequence, Subproblem (SP1) is not convex. To cope with it, a classical solution is to reformulate the subproblem into a convex one by means of transformation, which is the focus of the following work.

In Subproblem (SP1), ε_i is influenced by both WPT phase and WIT phase, which poses challenges for the convexity investigation of the object function. If ε_i is only affected by either of the two phases, the problem will be much more tractable. Moreover, it is obvious that the WIT ability is completely decided by the energy acquired during WPT phase, which implies an energy supply and consumption limitation. This motivates us to decouple the complicated nonlinear relationship between the ε_i and $\boldsymbol{P}$ during WPT phase and introduce sensor transmit power $\bar{\boldsymbol{P}}$ during WIT phase as a set of variables to be optimized with the objective of establishing a direct coupling relationship between ε_i and $\bar{P}_i$, which has the following advantages. First, the nonlinear relationship between γ_i and $\boldsymbol{P}$ has been replaced by a simple linear relationship between γ_i and $\bar{P}_i$, i.e.,$\gamma_i(\bar{P}_i) = \frac{\bar{P}_i\bar{z}_{2,i}}{\sigma_i^2}$. Based on such linear relationship, the convexity of ε_i with respect to $\bar{P}$ can easily obtained according to [42], in which the convex relationship between ε_i and SNR γ_i has been demonstrated. Second, the original equality relationship between $\bar{P}$ and $\boldsymbol{P}$, i.e., (12) has been converted to an inequality one, i.e., $\bar{P}_i \leq F_{eh}[\boldsymbol{Q}_i(\hat{\boldsymbol{P}})]\frac{n_0}{n_i}$, which facilitates the further utilization of SCA algorithm. As a result, with the introduction of optimization variables $\bar{\boldsymbol{P}}$, the problem is reformulated as:

$$\begin{aligned}
(\text{SP3}): \min_{\boldsymbol{P},\bar{\boldsymbol{P}}} \max_{i\in\{1,\ldots,N\}} \quad & \varepsilon_i(\bar{P}_i) && \text{(13a)}\\
s.t.\ & \bar{P}_i \leq F_{eh}[\boldsymbol{Q}_i(\boldsymbol{P})]\frac{n_0}{n_i}, && \text{(13b)}\\
& \frac{\bar{P}_i\bar{z}_{2,i}}{\sigma_i^2} \geq 1, && \text{(13c)}\\
& \frac{k_i}{n_i} - \log_2\left(1 + \frac{\bar{P}_i\bar{z}_{2,i}}{\sigma_i^2}\right) \leq 0, \\
& (9d), (9e). && \text{(13d)}
\end{aligned}$$

It is worthwhile mentioning that the optimal $(\bar{\boldsymbol{P}}^\star, \hat{\boldsymbol{P}}^\star)$ of problem (SP3) satisfies $\bar{P}_i^\star = F_{eh}[\boldsymbol{Q}_i(\hat{\boldsymbol{P}}^\star)]\frac{n_0}{n_i}$, which can be proved by the contradiction method due to the fact that the transmission error probability of sensor i is monotonically decreasing in the SNR $\gamma_i = \frac{\bar{z}_{2,i}}{\sigma^2}\bar{P}_i$, i.e., ε_i is monotonically decreasing in $\bar{P}_i$ with given $\bar{z}_{2,i}$ and σ^2. It indicates that problem (SP3) with slacked variables $\bar{\boldsymbol{P}}$ and slacked constraint (13b) is equivalent to (SP1). Subsequently, let us focus on (13b), which depicts the coupling energy supply and consumption constraint between WPT and WIT phase. According to the results conducted in our previous work [38], it has been proved that the joint convex property of $F_{eh}[\boldsymbol{Q}_i(\boldsymbol{P})]$ with respect to the reciprocal of multiple source power, i.e., $\frac{1}{\boldsymbol{P}}$. To facilitate the characterization, we define $\hat{\boldsymbol{P}} \triangleq \{\hat{P}_1, \hat{P}_2, \ldots, \hat{P}_{\mathrm{M}}\}$, where $\hat{P}_j = \frac{1}{\bar{P}_j}, \forall j \in \{1, \ldots, M\}$. Hence, the harvested power at sensor i, i.e., $F_{eh}[\boldsymbol{Q}_i(\boldsymbol{P})]$ is jointly convex in $\hat{\boldsymbol{P}}$. Based on the results, we perform variable substitutions to constraint (13b), (9d) and (9e), which are respectively reformed as

$$\bar{P}_i \leq F_{eh}[\boldsymbol{Q}_i(\hat{\boldsymbol{P}})]\frac{n_0}{n_i}, \tag{14}$$

$$\sum_{j=1}^{M} \frac{1}{\hat{P}_j} \leq P_{total}, \tag{15}$$

$$\hat{P}_j \geq \frac{1}{P_{max}}. \tag{16}$$

Nevertheless, the constraint (14) is nonconvex due to the nonconcave term $F_{eh}[\boldsymbol{Q}_i(\hat{\boldsymbol{P}})]$. To cope with it, we apply SCA

algorithm to convert the original non-convex constraint into a convex one. Based on the joint convexity of $F_{eh}[\boldsymbol{Q}_i(\hat{\boldsymbol{P}})]$ with respect to $\hat{\boldsymbol{P}}$, for any feasible local point $\hat{\boldsymbol{P}}^{(\tau)}$, we have

$$Q_{ch,i} = F_{eh}[\boldsymbol{Q}_i(\hat{\boldsymbol{P}})] \geq \sum_{j=1}^{M} -A_{i,j}^{(\tau)}\hat{P}_j + B_i^{(\tau)}, \tag{17}$$

where the equality holds when $\hat{\boldsymbol{P}} = \hat{\boldsymbol{P}}^{(\tau)}$, i.e., a tight approximation is achieved. Both $A_{i,j}^{(\tau)}$ and $B_i^{(\tau)}$ are the positive constants defined as

$$A_{i,j}^{(\tau)} = \frac{\partial F_{eh}[\boldsymbol{Q}_i(\hat{\boldsymbol{P}})]}{\partial \hat{P}_j} \mid_{\hat{P}_j=\hat{P}_j^{(\tau)}}, \tag{18}$$

$$B_j^{(\tau)} = F_{eh}[\boldsymbol{Q}_i(\hat{\boldsymbol{P}})] \mid_{\hat{P}_j=\hat{P}_j^{(\tau)}} + \sum_{j=1}^{M} A_{i,j}^{(\tau)}\hat{P}_j. \tag{19}$$

The non-concave term $F_{eh}[\boldsymbol{Q}_i(\boldsymbol{P})]$ has been approximated to a concave one $\sum_{j=1}^{M} -A_{i,j}^{(\tau)}\hat{P}_j + B_i^{(\tau)}$ and the Local Problem (LP1) based on any feasible point $\hat{\boldsymbol{P}}^{(\tau)}$ is given as

$$(\text{LP1}): \min_{\hat{\boldsymbol{P}},\bar{\boldsymbol{P}}} \max_{i\in\{1,\ldots,N\}} \varepsilon_i(\bar{P}_i) \tag{20a}$$

$$s.t.\ \bar{P}_i \leq \frac{n_0}{n_i}\left(\sum_{j=1}^{M} -A_{i,j}^{(\tau)}\hat{P}_j + B_i^{(\tau)}\right),$$
$$(13c), (15), (16). \tag{20b}$$

Obviously, all the constraints are convex. Subsequently, we investigate the convexity of the object function in Local Problem (LP1). In [38], the joint convexity of ε_i in $(\hat{\boldsymbol{P}}, \bar{\boldsymbol{P}})$ has been verified. Based on the convexity preservation, the maximum of a set of convex functions is still convex, which indicates the convexity of the objective function in (LP1), i.e., $\max_{i\in\{1,\ldots,N\}} \varepsilon_i(\bar{P}_i)$ is jointly convex to $(\hat{\boldsymbol{P}}, \bar{\boldsymbol{P}})$. As a result, Local Problem (LP1) is convex and can be effectively solved via convex programming methods.

C. SOLUTION TO SUBPROBLEM (SP2)

In this subsection, we address the Subproblem (SP2) (blocklength allocation problem) while the transmitted power from multiple WPT sources are given. In particular, we first investigate the convexity of error probability ε_i with respect to short packet transmission blocklength n_i. Subsequently, SCA algorithm is utilized for nonconvex constraint reformulation. Finally, a sub-optimal solution can be achieved through an iteration-based algorithm.

To verify the convexity of Subproblem (SP2), we first study the convexity of the object function in Subproblem (SP2). In particular, we propose the following Lemma 1 to assist the convexity confirmation of the object function.

Lemma 1: Under a total WPT energy constraint, the transmission error probability ε_i is convex in the transmission blocklength n_i while satisfying $\gamma_i \geq 1, r \geq 0.0683$[bits/ch.use], which is true for most practical FBL applications in the region of interest.

Proof: To facilitate the derivation, we define $x_i(n_i) = \sqrt{\frac{n_i}{(1-\frac{1}{\left(1+\frac{\zeta_i}{n_i}\right)^2})}}\left(\log_2\left(1+\frac{\zeta_i}{n_i}\right)-\frac{k_i}{n_i}\right)\ln 2$, based on which the transmission error probability from sensor i to the destination node can be written as $\varepsilon_i(n_i) = Q(x_i(n_i))$, where Q denotes the Q-function. To investigate the convexity of ε_i, we take the second derivative of ε_i with respect to n_i and judge the nonnegativity of it:

$$\frac{\partial \varepsilon_i}{\partial n_i} = \frac{\partial \varepsilon_i}{\partial x_i}\frac{\partial x_i}{\partial n_i}, \tag{22}$$

$$\frac{\partial^2 \varepsilon_i}{\partial n_i^2} = \frac{\partial^2 \varepsilon_i}{\partial x_i^2}\left(\frac{\partial x_i}{\partial n_i}\right)^2 + \frac{\partial \varepsilon_i}{\partial x_i}\frac{\partial^2 x_i}{\partial n_i^2}, \tag{23}$$

where $\frac{\partial^2 \varepsilon_i}{\partial x_i^2} = \frac{1}{\sqrt{2\pi}}x_i e^{-\frac{x_i^2}{2}} \geq 0$, $\left(\frac{\partial x_i}{\partial n_i}\right)^2 \geq 0$, $\frac{\partial \varepsilon_i}{\partial x_i} = -\frac{1}{\sqrt{2\pi}}e^{-\frac{x_i^2}{2}} < 0$. Nevertheless, the nonnegativity of term $\frac{\partial^2 x_i}{\partial n_i^2}$ cannot be easily obtained, which makes the nonnegativity of $\frac{\partial^2 \varepsilon_i}{\partial n_i^2}$ unpredictable. Therefore, the following work focuses on the nonnegatively proof of term $\frac{\partial^2 x_i}{\partial n_i^2}$ when $\gamma_i \geq 1$ and $r \geq 0.0683$[bits/ch.use] holds.

To facilitate the derivation, we define $x_i = \ln 2(\phi_i\psi_i)$, where $\phi_i = \sqrt{\frac{n_i}{\left(1-\frac{1}{(1+\frac{\zeta_i}{n_i})^2}\right)}}$ and $\psi_i = \left(\log_2(1+\frac{\zeta_i}{n_i})-\frac{k}{n_i}\right)$. The first-order derivative of ϕ_i and ψ_i can respectively be given as

$$\frac{\partial \phi_i}{\partial n_i} = \frac{(\zeta_i+n_i)(\zeta_i^2+3\zeta_i n_i+4n_i^2)}{2\zeta_i(\zeta_i+2n_i)^2\sqrt{\frac{n_i(\zeta_i+n_i)^2}{\zeta_i^2+2\zeta_i n_i}}}, \tag{24}$$

$$\frac{\partial \psi_i}{\partial n_i} = \frac{-\zeta_i n_i + \ln 2k_i(\zeta_i+n_i)}{n_i^2(\zeta_i+n_i)\ln 2}. \tag{25}$$

Based on (24) and (25), the first-order derivative of x_i with respect to n_i is given as:

$$\begin{aligned}\frac{\partial x_i}{\partial n_i} &= \ln 2\left(\frac{\partial \phi_i}{\partial n_i}\psi_i + \phi_i\frac{d\psi_i}{\partial n_i}\right)\\ &= \ln 2\Bigg(\underbrace{\frac{1}{2\zeta_i}\sqrt{\frac{\zeta_i}{n_i}}\frac{(\zeta_i^2+3\zeta_i n_i+4n_i^2)}{(\zeta_i+2n_i)^{\frac{3}{2}}}\left(\log_2(1+\frac{\zeta_i}{n_i})-\frac{k}{n_i}\right)}_{\omega_i}\\ &\quad + \underbrace{\frac{\sqrt{n_i}}{\sqrt{\zeta_i^2+2\zeta_i n_i}}\frac{-\zeta_i n_i+\ln 2k_i(\zeta_i+n_i)}{n_i^2\ln 2}}_{\rho_i}\Bigg)\end{aligned} \tag{26}$$

To facilitate the investigation of the second-order derivative of x_i with respect to n_i, we first take the first-order derivative of component ρ_i and ω_i with respect to n_i, i.e., $\frac{\partial \rho_i}{\partial n_i}$ and $\frac{\partial \omega_i}{\partial n_i}$,

which are given as follows.

$$\begin{aligned}\frac{\partial \rho_i}{\partial n_i} &= \frac{1}{2}\frac{\sqrt{\zeta_i(\zeta_i+2n_i)}}{(\zeta_i+2n_i)^2\sqrt{n_i}}\frac{-\zeta_i n_i+\ln 2k_i(\zeta_i+n_i)}{n_i^2} \\ &\quad+\sqrt{\frac{n_i}{\zeta_i^2+2\zeta_i n_i}}\frac{\zeta_i n_i-\ln 2k_i n_i-2\ln 2k_i\zeta_i}{n_i^3} \\ &= \frac{\frac{1}{2}\zeta_i^2 n_i-\frac{3}{2}\ln 2k_i\zeta_i^2+2\zeta_i n_i^2-\frac{9}{2}\zeta_i k_i n_i-2\ln 2k_i n_i^2}{\zeta_i n_i^2\sqrt{\frac{n_i}{\zeta_i^2+2\zeta_i n_i}}(\zeta_i+2n_i)^2}.\end{aligned} \tag{27}$$

$$\frac{\partial \omega_i}{\partial n_i} = \frac{\xi_i}{\varrho_i}, \tag{28}$$

where ξ_i and ϱ_i are respectively given as:

$$\begin{aligned}\xi_i &= (\zeta_i+n_i)^2 16\, k_i n_i^4\ln 2-2\zeta_i^4 n_i-20\zeta_i^2 n_i^3-10\zeta_i^3 n_i^2 \\ &\quad-16\zeta_i n_i^4-\zeta_i^4 n_i\ln\left(1+\frac{\zeta_i}{n_i}\right)-5\zeta_i^2 n_i^3\ln\left(1+\frac{\zeta_i}{n_i}\right) \\ &\quad-6\zeta_i^3 n_i^2\ln\left(1+\frac{\zeta_i}{n_i}\right)+3\zeta_i^4 k_i\ln 2+36\zeta_i k_i n_i^3\ln 2 \\ &\quad+18\zeta_i^3 k_i n_i\ln 2+35\zeta_i^2 k_i n_i^2\ln 2,\end{aligned} \tag{29}$$

$$\varrho_i = 4\zeta_i^2 n_i\ln 2(\zeta_i+2n_i)^4\left(\frac{n_i^3+2\zeta_i n_i^2+\zeta_i^2 n_i}{\zeta_i^2+2\zeta_i n_i}\right)^{3/2}. \tag{30}$$

Subsequently, the second-order derivative of x_i with respect to n_i can be obtained as (21), shown at the bottom of the page. Obviously, the denominator of $\frac{d^2x_i}{dn_i^2}$ is positive. Subsequently, we focus on the molecules in (21), which is defined as f in (31), shown at the bottom of the next page. Considering $\frac{\zeta_i}{n_i}=\gamma_i, \frac{k_i}{n_i}=r_i, f$ can further be reformulated to (32), as shown at the bottom of the next page. When $\gamma_i\geq 1, r_i\geq 0$ holds, ϵ_3 and ϵ_5 in (32) are non-negative terms and respectively satisfy:

$$\epsilon_3 \geq 8\ln(1+\gamma_i)+18\ln 2r_i-4]\gamma_i^2+6\ln 2r_i\gamma_i, \tag{34}$$

$$\epsilon_5 \geq [\ln(1+\gamma_i)+3\ln 2r_i]\gamma_i^2 \tag{35}$$

Moreover, term ϵ_2 satisfies:

$$\epsilon_2 \geq [18\ln(1+\gamma_i)+75\ln 2r_i\gamma_i^3-16]\gamma_i^3+3\ln 2r_i\gamma_i. \tag{36}$$

Based on the relaxation of term ϵ_2,ϵ_3 and ϵ_5, i.e., (34) (35) (36), we have the inequality function (33), as shown at the bottom of the next page. When $\gamma_i\geq 1$ and $r_i\geq 0.0683$ holds, ν_1, ν_2 and ν_3 respectively satisfies $\nu_1\geq 0.0039$,$\nu_2\geq 0.0273$ and $\nu_3\geq 0.0106$, which indicates that $f\leq 0$, thus $\frac{d^2x_i}{dn_i^2}\leq 0$ holds.

As a result, we have

$$\frac{\partial^2\varepsilon_i}{\partial n_i^2} = \left(\frac{1}{\sqrt{2\pi}}x_i e^{-\frac{x_i^2}{2}}\right)\left(\frac{\partial x_i}{\partial n_i}\right)^2-\left(\frac{1}{\sqrt{2\pi}}e^{-\frac{x_i^2}{2}}\right)\frac{\partial^2 x_i}{\partial n_i^2}\geq 0, \tag{37}$$

i.e., ε_i is convex with respect to n_i. □

With the assistance of Lemma 1, the convexity of the object function in Subprobelm (SP2), i.e., the joint convexity of $\max\varepsilon_i, i\in\{1,\ldots,N\}$ with respect to $\boldsymbol{n}$ can easily be proved as follows. Noted that ε_i denotes the error probability of the transmission of the $i-th$ packet, which is completely affected by the blocklength allocated to sensor i and is independent from the blocklength allocated to sensor i', $i\neq i'$, i.e., $\frac{\partial^2\varepsilon_i}{\partial n_{i'}^2}=0, \frac{\partial^2\varepsilon_i}{\partial n_i\partial n_{i'}}=0, i\neq i'$. Therefore, the Hessian matrix of ε_i with respect to $\boldsymbol{n}$ can be obtained as

$$\begin{bmatrix} \frac{\partial^2\varepsilon_i}{\partial n_1^2} & \cdots & \frac{\partial^2\varepsilon_i}{\partial n_1\partial n_i} & \cdots & \frac{\partial^2\varepsilon_i}{\partial n_1\partial n_N} \\ \vdots & \ddots & \vdots & \cdots & \vdots \\ \frac{\partial^2\varepsilon_i}{\partial n_i\partial n_1} & \cdots & \frac{\partial^2\varepsilon_i}{\partial n_i^2} & \cdots & \frac{\partial^2\varepsilon_i}{\partial n_i\partial n_N} \\ \vdots & \vdots & \vdots & \ddots & \vdots \\ \frac{\partial^2\varepsilon_i}{\partial n_N\partial n_1} & \cdots & \frac{\partial^2\varepsilon_i}{\partial n_N\partial n_i} & \cdots & \frac{\partial^2\varepsilon_i}{\partial n_N^2} \end{bmatrix} = \begin{bmatrix} 0 & \cdots & 0 & \cdots & 0 \\ \vdots & \ddots & \vdots & \cdots & \vdots \\ 0 & \cdots & \frac{\partial^2\varepsilon_i}{\partial n_i^2} & \cdots & 0 \\ \vdots & \vdots & \vdots & \ddots & \vdots \\ 0 & \cdots & 0 & \cdots & 0 \end{bmatrix},$$

which is clearly positive semi-definite. Thus, ε_i is jointly convex in $\boldsymbol{n}$. Based on the convexity preservation, the maximum of a set of convex functions is still convex, i.e., $\max\ \varepsilon_i(n_i), i\in\{1,\ldots,N\}$ is also jointly convex in $\boldsymbol{n}$.

So far, the convexity of the object function in Subproblem (SP2) has been characterized. The following task is to prove the convexity of the constraints in Subproblem (SP2). Constraint (11b) is nonconvex, but can be easily transferred into a convex one, i.e., $\zeta_i\geq n_i$. Constraint (11d) is linear, which is also convex. Nevertheless, constraitn (11c) is nonconvex due to the non-concave term $\log_2(1+\frac{\zeta_i}{n_i})$. To cope with it, we utilize the same method in IV-B, i.e., SCA to convert the non-concave term $\log_2(1+\frac{\zeta_i}{n_i})$ into a concave one. The

$$\begin{aligned}\frac{\partial^2 x_i}{\partial n_i^2} &= \ln 2\left(\frac{\partial\omega}{\partial n_i}+\frac{\partial\rho}{\partial n_i}\right) \\ &= \ln 2\Bigg(8\zeta_i n_i^5+20\zeta_i^2 n_i^4+16\zeta_i^3 n_i^3+4\zeta_i^4 n_i^2-24k_i\zeta_i^5\ln 2-5\zeta_i n_i^5\ln\left(1+\frac{\zeta_i}{n_i}\right)-\zeta_i^5 n_i\ln\left(1+\frac{\zeta_i}{n_i}\right). \\ &\quad-16\zeta_i^2 n_i^4\ln\left(1+\frac{\zeta_i}{n_i}\right)-18\zeta_i^3 n_i^3\ln\left(1+\frac{\zeta_i}{n_i}\right)-8\zeta_i^4 n_i^2\ln\left(1+\frac{\zeta_i}{n_i}\right)-3\zeta_i^5 k_i\ln 2-87\zeta_i k_i n_i^4\ln 2 \\ &\quad-24\zeta_i^4 k_i n_i\ln 2-120\zeta_i^2 k_i n_i^3\ln 2-78\zeta_i^3 k_i n_i^2\ln 2\Bigg)\Bigg/\left(4\zeta_i n_i\ln 2(\zeta_i+2n_i)^4\left(\frac{n_i^3+2\zeta_i n_i^2+\zeta_i^2 n_i}{\zeta_i^2+2\zeta_i n_i}\right)^{3/2}\right)\end{aligned} \tag{21}$$

second-derivation of $\log_2(1+\frac{\zeta_i}{n_i})$ with respect to n_i is given as $\frac{\partial^2(\log_2(1+\frac{\zeta_i}{n_i}))}{\partial n_i^2} = \frac{2\zeta_i n_i+\zeta_i^2}{\ln 2(n_i+\zeta_i)^2 n_i^2}$, which is non-negative with $\zeta_i \geq 0, n_i \geq 0$. Therefore, $\log_2(1+\frac{\zeta_i}{n_i})$ is convex in n_i. Based on the convexity of $\log_2(1+\frac{\zeta_i}{n_i})$, an inequality can be obtained as follows.

$$\log_2\left(1+\frac{\zeta_i}{n_i}\right) \geq -C_i^{(\chi)} n_i + D_i^{(\chi)}, \tag{38}$$

where $C_i^{(\chi)}$ and $D_i^{(\tau)}$ are defined as

$$C_i^{(\chi)} = -\frac{d\left(\log_2\left(1+\frac{\zeta_i}{n_i}\right)\right)}{dn_i} \Big|_{n_i=n_i^{(\chi)}}, \tag{39}$$

$$D_i^{(\chi)} = \log_2\left(1+\frac{\zeta_i}{n_i}\right) \Big|_{n_i=n_i^{(\chi)}} + C_i^{(\chi)} n_i. \tag{40}$$

The equality in (38) holds at local point $\boldsymbol{n}^{(\chi)}$. Based on the SCA, the original nonconcave term $\log_2(1+\frac{\zeta_i}{n_i})$ has been converted into a linear and concave one, i.e., $-C_i^{(\chi)} n_i + D_i^{(\chi)}$. In the χ-th iteration, the local-problem is written as

$$\begin{aligned}
(\text{LP2}): \min_{\{\mathbf{n}\}} \ & \sum_{i=1}^{N} \varepsilon_i && \text{(41a)}\\
s.t.: \ & \zeta_i \geq n_i, && \text{(41b)}\\
& \frac{k_i}{n_i} \leq -C_i^{(\chi)} n_i + D_i^{(\chi)}, && \text{(41c)}\\
& \sum_{i=1}^{N} n_i \leq N_{total}, && \text{(41d)}
\end{aligned}$$

which is a convex problem and can be effectively solved by convex optimization tools.

D. SOLUTION TO ORIGINAL PROBLEM (OP)

By alternately addressing the two decomposed problems, i.e., Subproblem (SP1) and (SP2), which have been effectively solved in IV-B and IV-C, we can obtain a suboptimal solution to the original problem. The joint power and blocklength allocation algorithm is depicted in Alforithm 1. In particular, we first initialize the values of $\left(\boldsymbol{P}^{(0)}, \bar{\boldsymbol{P}}^{(0)}, \boldsymbol{m}^{(0)}\right)$ and calculate the corresponding initialized maximum error probability. Subsequently, the alternating of two subproblems is started. The power allocation problem is first addressed. In the τ-th iteration for power allocation problem settlement, we address the Local Problem (LP1) and obtain the corresponding optimal solution $\left(\hat{\boldsymbol{P}}^{(\tau)}, \bar{\boldsymbol{P}}^{(\tau)}\right)$, based on which a new local problem arises accordingly. The iteration progresses until the result converges. Finally, a suboptimal solution to Subproblem (SP1) is obtained. Based on the obtained multiple WPT sources power allocation results, blocklength allocation problem, i.e., Subproblem (SP2) is subsequently addressed. Similar to the power allocation algorithm, in the χ-th iteration, we first determine $C_i^{(\chi)}, D_i^{(\chi)}$, and subsequently solve the Local Probelm (LP2). After repetition, we can obtain a suboptimal solution to the blocklength allocation problem, which also represents the end of a round of alternation between power and blocklength allocation. Subsequently, a new round of alternation starts, in which the power and blocklength allocation results obtained in the previous round of alternation are taken as the initial values. Such iterations proceeds until the results converges.

Lastly, we study the complexity of the proposed iteration algorithm based on the ellipsoid method. Sub Problem (SP1) has $(M+N)$ optimization variables, which leads to $\mathcal{O}\left((M+N)^2\frac{1}{\epsilon}\right)$ rounds of ellipsoid updates, where ϵ denotes the optimization threshold. With each cycle of ellipsoid updating, the complexity cost for object function is $\mathcal{O}\left((M+N)^2\right)$ and that for constraints is $\mathcal{O}\left((M+N)(N+N+M+1)\right)$. As a result, with Φ rounds of iteration, the complexity of the power allocation algorithm can be given as $\mathcal{O}\left(\Phi(M+N)^2\frac{1}{\epsilon}\right)\times\left(\mathcal{O}(M+N)^2+\mathcal{O}\left((M+\right.\right.$

$$\begin{aligned}
f = \ln 2\, n_i^6 \Bigg(& 8\frac{\zeta_i}{n_i} + 20\left(\frac{\zeta_i}{n_i}\right)^2 + 16\left(\frac{\zeta_i}{n_i}\right)^3 + 4\left(\frac{\zeta_i}{n_i}\right)^4 - 24\ln 2\frac{k_i}{n_i} - 5\frac{\zeta_i}{n_i}\ln\left(1+\frac{\zeta_i}{n_i}\right) - \left(\frac{\zeta_i}{n_i}\right)^5 \ln\left(\frac{\zeta_i+n_i}{n_i}\right)\\
& -16\left(\left(\frac{\zeta_i}{n_i}\right)^2 \ln\left(1+\frac{\zeta_i}{n_i}\right)\right) - 18\left(\frac{\zeta_i}{n_i}\right)^3 \ln\left(1+\frac{\zeta_i}{n_i}\right) - 8\left(\frac{\zeta_i}{n_i}\right)^4 \ln\left(1+\frac{\zeta_i}{n_i}\right) - 3\ln 2\left(\frac{\zeta_i}{n_i}\right)^5 \frac{k_i}{n_i}\\
& -87\ln 2\frac{\zeta_i}{n_i}\frac{k_i}{n_i} - 24\ln 2\left(\frac{\zeta_i}{n_i}\right)^4 \frac{k_i}{n_i} - 120\ln 2\left(\frac{\zeta_i}{n_i}\right)^2 \frac{k_i}{n_i} - 78\ln 2\left(\frac{\zeta_i}{n_i}\right)^3 \frac{k_i}{n_i}\Bigg),
\end{aligned} \tag{31}$$

$$\begin{aligned}
f = -\ln 2 n_i^6 \Big\{ & \underbrace{[16\ln(1+\gamma_i) + 120\ln 2r_i - 20]\gamma_i^2}_{\epsilon_1} + \underbrace{[18\ln(1+\gamma_i) + 78\ln 2r_i\gamma_i^3 - 16]\gamma_i^3}_{\epsilon_2}\\
& + \underbrace{[8\ln(1+\gamma_i) + 24\ln 2r_i - 4]\gamma_i^4}_{\epsilon_3} + \underbrace{[5\ln(1+\gamma_i) + 87\ln 2r_i - 8]\gamma_i}_{\epsilon_4} + \underbrace{[\ln(1+\gamma_i) + 3\ln 2r_i]\gamma_i^5}_{\epsilon_5} + 24\ln 2r_i\Big\}.
\end{aligned} \tag{32}$$

$$f \leq -\ln 2 n_i^6 \Big\{ \underbrace{[25\ln(1+\gamma_i) + 141\ln 2r_i - 24]}_{\nu_1}\gamma_i^2 + \underbrace{[18\ln(1+\gamma_i) + 75\ln 2r_i\gamma_i^3 - 16]}_{\nu_2}\gamma_i^3 + \underbrace{[5\ln(1+\gamma_i) + 96\ln 2r_i - 8]}_{\nu_3}\gamma_i\Big\} \tag{33}$$

Algorithm 1 Joint Resource Allocation Algorithm

Initialization

1) Initialize the feasible $(\boldsymbol{P}^{(0)}, \bar{\boldsymbol{P}}^{(0)}, \boldsymbol{m}^{(0)})$.

2) Initialize the maximum error probability $\boldsymbol{\varepsilon}_{\max}{}^{(0)}$ based on $(\boldsymbol{P}^{(0)}, \bar{\boldsymbol{P}}^{(0)}, \boldsymbol{m}^{(0)})$.

Joint Resource Allocation

3)Initialize $\varepsilon_{\text{joint}} = \varepsilon_{\max,\min} = \varepsilon_{\max}^{(0)}$, $\boldsymbol{P}_{opt} = \boldsymbol{P}^{(0)}$, $\bar{\boldsymbol{P}}_{opt} = \bar{\boldsymbol{P}}^{(0)}$,
$\boldsymbol{m}_{opt} = \boldsymbol{m}^{(0)}$, $\varkappa = 0$.

4)Iteration $\varkappa = \varkappa + 1$

Power Allocation

5) Initialize $\hat{\boldsymbol{P}} = 1/\boldsymbol{P}_{opt}$, $\tau = 0$.
for sensor $i = 1 : N$
for source $j = 1 : M$

6) Determine parameters $A_{ij}^{(\tau)}$ according to (18)
endfor

7) Determine parameters $B_i^{(\tau)}$ according to (19)
endfor

8) Update $(\hat{\boldsymbol{P}}^{(\tau+1)}, \bar{\boldsymbol{P}}^{(\tau+1)})$ by solving (18)

9) **if** $\left|\varepsilon_{\max}^{(\tau+1)} - \varepsilon_{\max,\min}\right| / \varepsilon_{\text{o,min}} \leq \varepsilon_{\text{converge-threshold}}$
$\boldsymbol{P}^{(\varkappa)} = 1/\hat{\boldsymbol{P}}^{(\tau+1)}$
break
endif

10) **if** $\varepsilon_{\max}^{(\tau+1)} < \varepsilon_{\max,\min}$
$\varepsilon_{\max,\min} = \varepsilon_{\max}^{(\tau+1)}$, $\hat{\boldsymbol{P}}_{opt} = \hat{\boldsymbol{P}}^{(\tau+1)}$,$\boldsymbol{P}_{opt} = 1/\hat{\boldsymbol{P}}^{(\tau+1)}$
endif

11) $\tau = \tau + 1$ and jump to step b).

Blocklength Allocation

12) Initialize $\chi = 0$
for sensor *i*=1:N

13) Determine $C_i^{(\chi)}$ and $D_i^{(\chi)}$ according to (39,40)
endfor

14) Update blocklength $n_i^{(\chi+1)}$ via solving (P4)

15) **if** $\left|\varepsilon_{\max}^{(\chi+1)} - \varepsilon_{\max,\min}\right| / \varepsilon_{\max,\min} \leq \varepsilon_{\text{converge-threshold}}$
$\varepsilon_{\text{joint}}^{\varkappa} = \varepsilon_{\max}^{(\chi+1)}$,$\boldsymbol{m}^{(\varkappa)} = \boldsymbol{m}^{(\chi+1)}$,
break
endif

16) **if** $\varepsilon^{(\chi+1)} < \varepsilon_{max,min}$
$\varepsilon_{max,min} = \varepsilon^{(\chi+1)}$, $\boldsymbol{n} = \boldsymbol{n}^{(\chi+1)}$,
endif

17) **if** $\left|\varepsilon_{\textbf{joint}}^{\varkappa} - \varepsilon_{\textbf{joint}}^{\varkappa-1}\right| / \varepsilon_{\textbf{joint}}^{\varkappa-1} \leq \varepsilon_{\textbf{converge-threshold}}$
break
else return to step 4)
endif

$N)(N+N+M+1)\Big) = \mathcal{O}\left(\Phi(M+N)^3(2M+3N+1)\frac{1}{\epsilon}\right) = \mathcal{O}\left(2\Phi(M+N)^4\frac{1}{\epsilon}\right)$. We can similarly obtain the complexity of the blocklength allocation algorithm as $\mathcal{O}\left(\Phi N^2\frac{1}{\epsilon}\right) \times \Big(\mathcal{O}(N^2)+\mathcal{O}\big(N(N+N+1)\big)\Big) = \mathcal{O}\left(\Phi 3N^4\frac{1}{\epsilon}\right)$. As a result, with ϖ rounds of alternating iterations, the complexity of the proposed joint resource allocation algorithm can be given as $\varpi \times \left(\mathcal{O}\left(\Phi(M+N)^3(M+2N)\frac{1}{\epsilon}\right) + \mathcal{O}\left(\Phi 3N^4\frac{1}{\epsilon}\right)\right)$.

V. NUMERICAL RESULTS

In this section, we first validate our joint resource allocation design in V-A and subsequently evaluate the system performance, including the impacts of diverse setups on reliability as well as the performance comparisons between our design and the benchmarkers in V-B. In simulation, the default parameters are setup as follows. With respect to the system topology, five sensors are deployed on a circle evenly with the center at the origin of the Cartesian coordinate, i.e., (0, 0) and the radius of the circle is set to 2 meters. The destination node is distributed at (15,15) in the Cartesian coordinate. Three WPT sources are deployed on an arc 20 meters away from the destination node and 5 meters from the center of multiple sensors. The blocklength is set as $n_0 = 500$, $n_{total} = 3000$. The packet size of all short packets are set to $k_i = 70$bits, $i \in \{1, \ldots, N\}$. For the nonlinear EH process, we have the following setup parameters based on [36]: $I_s = 5\mu A$, $\hat{R}_L = 200\Omega$, $n_0 = 4$. Moreover, the minimized maximum error probability is abbreviated as MMEP to facilitate the discussion.

A. VALIDATION

In this subsection, we first validate the proposed Lemma 1 and subsequently verify the efficiency of our proposed design. Finally, the necessity of the nonlinear EH model for practical design is validated.

1) VALIDATION OF LEMMA 1

We assume three sensors are deployed for short packet transmission and the available total blocklength for their transmission is limited to 1500 symbols. The relationship between the maximum error probability and n_1, n_2 has been depicted in Fig. 2 and Fig. 3 on the next page respectively in a linear-scale and logarithmic-scale. Obviously, the maximum error probability is jointly convex in the WIT blocklength of two sensors, which is consistent with the analytical results in lemma 1. Moreover, we can also observe that the maximum error probability among multiple short packet transmissions, in some cases, rarely changes when blocklength allocation decisions vary. For instance, when n_2 is set to 100 symbols, the maximum error probability does not change while n_1 varies from 100 to 500 symbols. It can be interpreted by the fact that MMEP is bottlenecked by the most unreliable transmission among all short packet transmissions and the sensor which is allocated with rather little resource has a huge probability of making a decisive impact on system reliability. This result indicates that a corresponding reasonable resource allocation plays a significant role in system reliability bottleneck enhancement.

2) CONVERGENCE BEHAVIOR OF PROPOSED ALGORITHM

Subsequently, we move on to evaluate the efficiency and accuracy of our proposed iteration-based joint resource

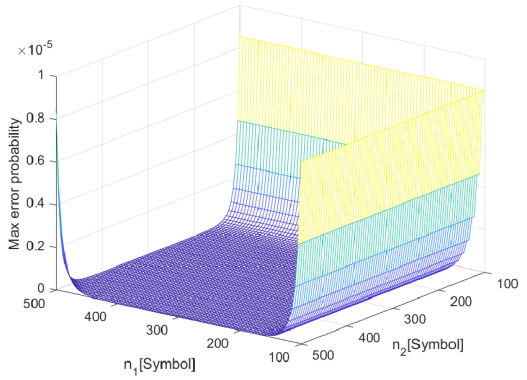

FIGURE 2. Joint convexity of maximum error probability with respect to multiple WIT blocklength in linear form.

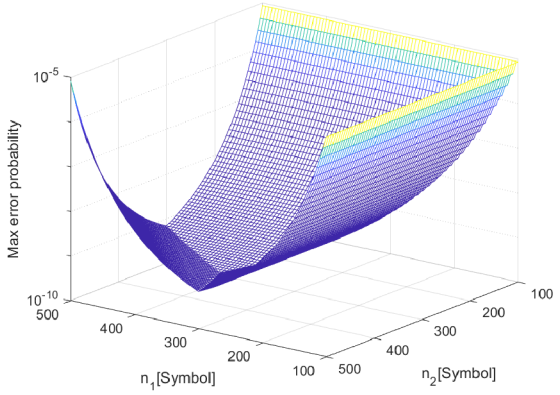

FIGURE 3. Joint convexity of maximum error probability with respect to multiple WIT blocklength in logarithm form.

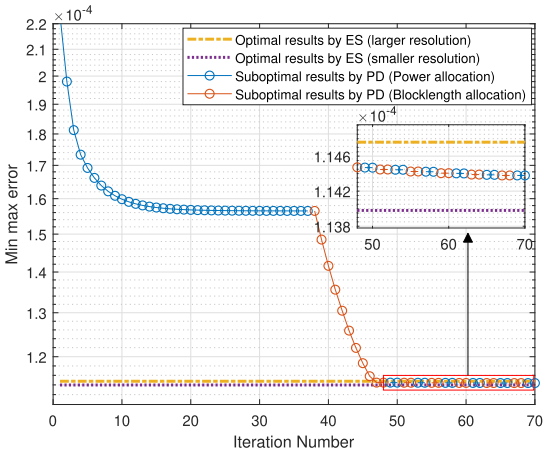

FIGURE 4. MMEP over iterations, where the results of both proposed design (PD) and exhaustive search (ES) are depicted.

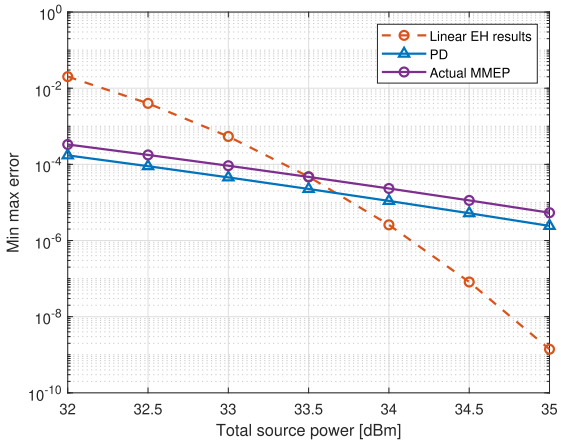

FIGURE 5. Results of power allocation design while diverse EH models (linear and nonlinear EH) are considered.

allocation algorithm. Optimal results obtained from exhaustive search (ES) algorithm with different resolutions are also provided. As shown in Fig. 4, power allocation and blocklength allocation are alternatively performed and the minimized maximum error probability (MMEP) decreases as the iteration progresses and finally converges. Obviously, two sharp reductions of MMEP respectively occur in the power and the blocklength allocation in the first round of optimization, subsequently the MMEP decreases slowly and approximately converges at the 50th iteration, which confirms the efficiency of our method. To investigate the accuracy of PD, the optimal result obtained from exhaustive search (ES) is also provided. We can observe that ES with smaller resolution helps to obtain a better resource allocation scheme compared to the large resolution results, resulting in a more reliable transmission, nevertheless, at the same time more time is consumed due to the larger searching space. By comparing 'PD' and 'ES (smaller resolution)', we can learn that the sub-optimal solution of PD is very close to the exhaustive search one with less than 10^{-7} amount of order error, which confirms the accuracy of PD. Although ES (smaller resolution) achieves relatively higher FBL reliability, its complexity is extremely significant, i.e., $\mathcal{O}\left((\frac{P_{total}}{P_{unit}})^{M-1} \times (\frac{n_{total}}{n_{unit}})^{N-1}\right)$, where P_{unit} and n_{unit} respectively denote the step length for power and blocklength searching. We can learn that the complexity of 'ES' is extremely higher than that of our algorithm $\varpi \times \left(\mathcal{O}\left(\Phi(M+N)^3(M+2N)\frac{1}{\epsilon}\right) + \mathcal{O}\left(\Phi 3N^4\frac{1}{\epsilon}\right)\right)$, especially with large M (source number) and N (sensor number). The result indicates that our algorithm appears to be both accurate and efficient. More interestingly, on the one hand, we can observe that the alternating iterations of power and blocklength are performed more than once, which suggests a correlation between power and blocklength, i.e., different power (or blocklength) setups corresponds to different blocklength (power) decisions for maximum error probability minimization, which emphasizes the significance of the joint resource optimization. On the other hand, one round of power-blocklength optimization has already yielded a result close to the optimal solution, which indicates that in practical design, a relatively good result can also be obtained via few rounds of power-blocklength optimization when multiple rounds of optimization are not allowed (e.g., extreme time-sensitive communication).

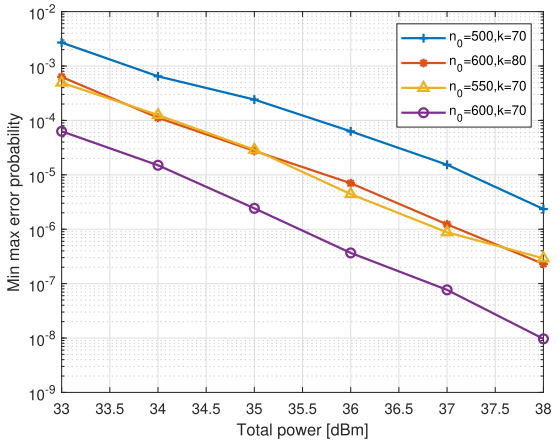

FIGURE 6. MMEP over total transmit power for multiple WPT sources with diverse WPT blocklength and packet size.

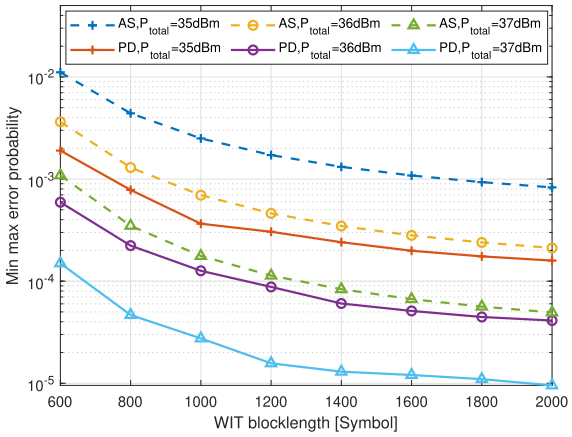

FIGURE 7. MMEP versus total WIT blocklength with diverse total source power setups, where resource average sharing design (ES) is utilized as benchmarker for performance advantage evaluation of the proposed design (PD).

3) NECESSITIES OF NONLINEAR EH MODEL

Next, we verify the importance of utilizing the nonlinear model to depict the EH process. In Figure 5, the MMEP results of power allocation under both linear and nonlinear EH models are provided, where 'LPA' and 'NPA' denote the power allocation results respectively based on the linear EH model and the nonlinear EH model. 'Actual MMEP' represents the practical MMEP of the 'LPA' algorithm, i.e., the power scheduling solutions obtained from 'LPA' are regarded as the transmit power of multiple WPT sources and the practical MMEP is accordingly calculated based on the practical nonlinear multi-RF signals combined EH model, i.e., (2). Obviously, when $P_{total} = 33.5\ dBm$, the theoretical result based on the linear model is close to its actual MMEP calculated by the nonlinear model. Nevertheless, when the total source power continuously increases or decreases from $33.5dBm$, significant performance gaps are observed between 'LPA' and 'Actual MMEP'. This result suggests that the linear EH model is too idealized for practical system design, since only within a narrow range does the linear EH model accurately depicts the practical situation. Moreover, we can learn that the slope of 'LPA' is significantly larger than that of the other two curves, which indicates that the FBL reliability based on linear EH model is much more sensitive to the total source power.

B. PERFORMANCES ANALYSIS AND COMPARISON

In this subsection, we investigate the impacts of diverse setups on the system reliability, including the total source power, WIT blocklength, packet size, sensor number and source number, etc. The performance advantage of our joint resource allocation design compared with the benchmarkers are also emphasized. Based on the numerical results, some suggestions are also provided for practical system design.

1) IMPACT OF TOTAL POWER ON MMEP

First of all, we study the impact of total power on the MMEP, where diverse WPT blocklength and packet size setups are assumed. In Fig 6, larger total power contributes to lower MMEP. In particular, more source power leads to more energy harvested by sensors, supporting short packets transmission with higher reliability. More interestingly, the slopes of all the curves rarely changes regardless of the amount of total power, which indicates that although energy acquisition is a nonlinear process, the total power has an approximately linear effect on the logarithm of the system's reliability and a relatively stable reliability performance enhancement can be achieved by enlarging the total source power. Moreover, we can learn that larger WPT blocklength and smaller packet size leads to lower MMEP. In particular, larger WPT blocklength represents longer EH duration, which indicates more available energy for short packet transmissions. The smaller packet size means lighter transmission burden, which requires relatively less resources for reliable transmission. In addition, it can be observed that curve '$n_0 = 550, k = 70$' and curve '$n_0 = 600, k = 80$' are close to each other. This result indicates that the system is capable of supporting reliable transmission of packet with larger data size by sacrificing a certain amount of transmission latency. From another perspective, in delay-sensitive applications, the size of the packet that the system can support to transfer is relatively reduced when a more strict delay requirements is announced.

2) IMPACT OF TOTAL WIT BLOCKLENGTH ON MMEP

We next investigate the impact of total WIT blocklength on the MMEP in Fig. 7. As expected, the MMEP is monotonically decreasing in the WIT blocklength. More interestingly, all the curves first drop sharply and subsequently flatten as the WIT blocklength increases. For one thing, based on (2), longer blocklength n directly contributes to lower error probability. For another thing, larger WIT blocklength results in lower SNR when the harvest energy is given, which makes a negative impact on system reliability. In other words, Fig. 7 also illustrates a tradeoff with respect to blocklength.

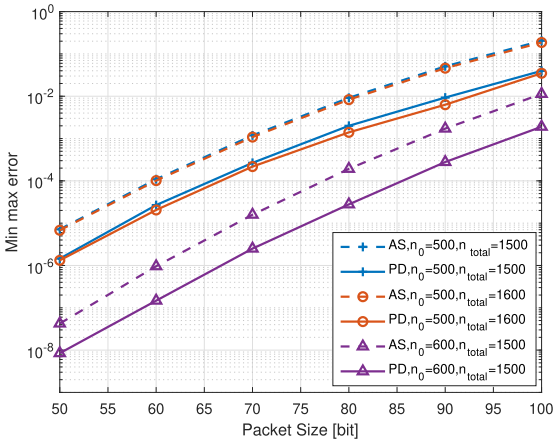

FIGURE 8. MMEP versus packet size with diverse WPT and WIT blocklength setups. The results of both PD and AS are provided.

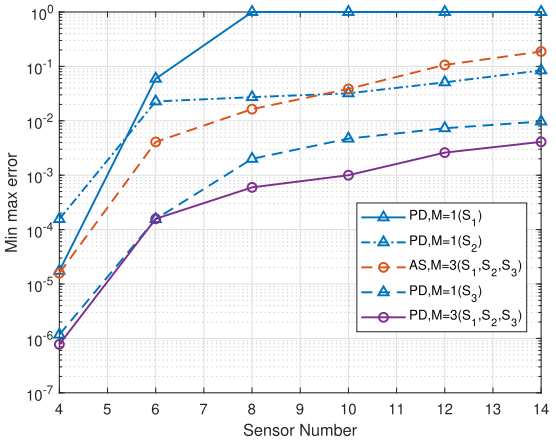

FIGURE 9. MMEP versus sensor number with diverse WPT sources deployments.

In addition, the results based on resource average sharing (AS) strategy is also provided as performance benchmarkers. We can learn that our 'PD' significantly outperforms the 'AS' and a stable reliability enhancement (compared with AS) is achieved regardless of the WIT blocklength, i.e., the reliability enhancement barely changes as WIT blocklength changes. When $P_{total} = 36dBm$, the MMEP of 'AS' with 2000 symbols as WIT blocklength is close to the MMEP of 'PD' with 800 WIT blocklength, i.e., to achieve a same MMEP, our PD is capable of reducing 60% of the transmission delay compared with 'AS'. By comparing 'PD, $P_{total} = 36dBm$' and 'AS, $P_{total} = 37dBm$', the 'PD' is observed to reach a higher system reliability with lower power consumption. This result indicates that a fuller utilization of the limited resources can be achieved by our 'PD'. Moreover, as P_{total} increases from 35dBm to 37dBm, a uniform reliability enhancement is achieved by both 'PD' and 'AS', which is consistent with the analysis in Fig. 6.

3) IMPACT OF PACKET SIZE ON MMEP

Subsequently, we analyze the impact of packet size on MMEP in Fig. 8. To facilitate the analysis, we assume that all sensors transmit short packets with same size. As shown in Fig. 8, larger packet size results in higher MMEP, which is consistent with the results in Fig. 6. Moreover, larger WPT blocklength n_0 or WIT blocklength n_{total} contributes to higher FBL reliability, which indicates that higher transmission reliability can be obtained by sacrificing a portion of the latency (i.e., longer blocklength). More interestingly, when additional latency is allowed in the system, (e.g., the total communication blocklength (n_0+n_{total}) increases 100 symbols from 2000 to 2100), extending the WPT phase (i.e., increasing n_0 from 500 to 600) results in higher reliability than extending the WIT phase (i.e., increasing n_{total} from 1500 to 1600) and a more significant performance enhancement can be achieved ('AS' as a benchmark). On the one hand, as discussed in Fig. 7, there exists a tradeoff with respect to the short packet transmission blocklength. The reduction in MMEP introduced by extending the WIT blocklength gradually diminishes as the blocklength increases. On the contrary, the reliability enhancement introduced by longer WPT blocklength is much more stable and significant. On the other hand, during WPT phase, multiple sources transmit RF signals to all sensors in a broadcasting manner, which indicates that all sensors can simultaneously benefit from the increase in n_0. Nevertheless, multiple sensors sequentially perform short packet transmission in a TDD mode during WIT phase. It indicates that there exists a blocklength resource competition among multi-sensors with the objective of guaranteeing their respective reliable transmissions, i.e., the performance advantages brought by the increased blocklength of WIT phase cannot be shared by all sensors. This result suggests to allocate relatively more time (blocklength) for the WPT phase for frame designs.

4) IMPACT OF SENSOR NUMBER ON MMEP

Subsequently, we move on to investigate the influence of sensor number on system reliability in Fig. 9. We can observe that more sensors result in higher MMEP since the blocklength assigned to each sensor shrinks as the sensor number enlarges, which results in lower system reliability. By comparing the 'PD' and 'AS', we can once again observe that our 'PD' significantly improves the system reliability and such performance enhancement gradually enlarges from around one order of magnitude to two orders of magnitude as the sensor number increases from 4 to 14, which indicates that reasonable power and blocklength joint optimization is of great significant, especially in applications with larger number of sensors. This result can be interpreted as the fact that in our defined scenario, more sensors would introduce greater heterogeneity, thus more significant flexibility for resource allocation and more potential for performance enhancement are introduced. In addition, reliability performances with diverse WPT source deployments are also provided. In scenario with a singular WPT source, the joint power and blocklength allocation design is equivalent to the pure blocklength allocation. Obviously, 3 sources (S_1, S_2, S_3) enabled WPCN

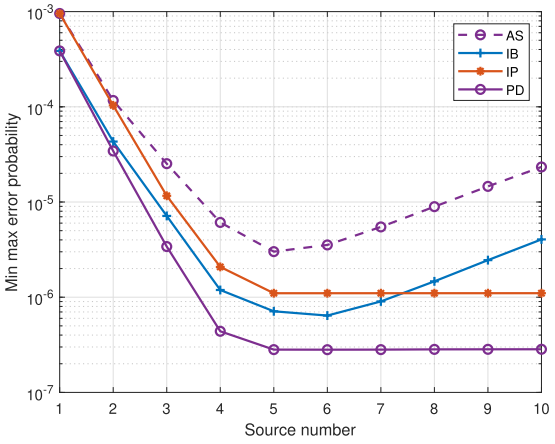

FIGURE 10. Comparison of system performance under diverse resource allocation regimes. MMEP versus source number is also provided.

significantly outperforms the one with only one singular WPT source (S_1 or S_2 or S_3). On the one hand, channel diversity introduced by multiple sources is capable of compensating deep fading, which can improve the system robustness for wireless powered communication. One the other hand, multiple sources introduce more flexibility for resource allocation and accordingly enables a more significant potential for performance enhancement. More interestingly, although multiple sources can bring numerous benefits for transmission that cannot be provide by a singular WPT source, the reliability of a multi-source WPCN is not necessarily better than that of a single-source WPCN. For instance, curve 'PD, M = 1(S3)' represents the pure blocklength allocation design in a single-source WPCN, which achieves higher FBL reliability than the average sharing resource allocation design in a multi-source WPCN, i.e., curve 'AS, M = 3(S1,S2,S2)'. The result indicates that the joint resource optimization among such multi-source driven WPCN plays a key role in performance improvement, which fully utilizes the advantages of multiple WPT sources. In addition, when the combined driving of multi-source is not possible in certain scenarios, the reasonable selection of the only WPT source can also help system to achieve a relatively reliable transmission.

5) IMPACT OF SOURCE NUMBER ON MMEP AND PERFORMANCE ANALYSIS OF INDEPENDENT POWER AND BLOCKLENGTH ALLOCATION.

To investigate the respective contribution of power allocation and blocklength allocation on system reliability performance enhancement in the joint resource optimization design, Fig. 10 depicts the MMEP versus diverse WPT source number under different resource allocation schemes, including average sharing strategy (AS), independent power allocation (IP), independent blocklength allocation (IB) as well as our proposed joint power and blocklength allocation design (PD). All WPT sources are arranged in a cluster along a straight line that traverses the area of several sensors. As the size of the source cluster increases, the number of WPT sources increases accordingly. By performance comparison, it is easy to notice that our PD significantly outperforms the other three resource allocation schemes (i.e., AS, IP, IB) and it is worth mentioning that such performance advantage i.e., the MMEP reduction of PD compared with other three schemes, becomes more significant when the number of WPT sources increases. This result indicates that the joint optimization of power and blocklength plays a crucial role in guaranteeing reliable short packet transmission, especially in scenarios where more WPT sources are jointly utilized as energy suppliers. Moreover, we can observe that when $M = 1$, i.e., only one WPT source is deployed, the obtained MMEP are the same for 'IP' and 'AS' and the same for 'IB' and 'PD'. This happens due to the fact that power allocation makes no sense with a singular WPT source, thus independent power allocation is equivalent to the average sharing regime. Similarly, the joint resource (power and blocklength) allocation design is equivalent to the independent blocklength allocation design. More interestingly, we can also observe that more WPT sources (larger source cluster) do not necessarily help achieve more reliable transmission if there is a lack of reasonable power allocation design. Specifically, for 'IB' and 'AS' regimes, larger WPT source number results in worse system reliability when $M \geq 6$. In contrast, the curves 'IP' and 'PD' do not trend upward, but rather flatten out. The reasons might be the following: On the one hand, a certain number of WPT sources may have already guaranteed a great coverage of all the sensors, i.e., all the sensors have received sufficient energy for short packet transmission. Therefore, the utilization of additional WPT sources may have rather less contribute for higher transmission reliability since the total available power among all the sources is limited. On the other hand, with given total power, a larger source cluster might do not have better power supply capabilities than the existing sources (e.g., due to the relatively isolated location), which not only limits the further reliability enhancement but even results in the potential to degrade the system performance. Taking 'AS' and 'IB' as instances, the transmit power of each source is decreased as the number of sources increases (due to the limited total transmit power among multiple sources), which makes the sources with better WPT performance not fully utilized and accordingly negatively affect the FBL reliability, which explains why the curves 'AS' and 'IB' tend to increase when the source number increases to a certain number. This result shows that both reasonable WPT source configuration and the corresponding resource scheduling are important factors for high reliability achievement in practical system designs.

VI. CONCLUSION

In this study, we investigated a multi-source enabled short packet transmission network, where the practical nonlinear EH model is considered. In particular, we characterized the FBL reliability in the multi-source WPCN. Considering the fairness among sensors, a joint power and blocklength allocation design targeting at minimizing the maximum error

probability among multiple short packet transmissions is accordingly proposed. Nevertheless, due to the nonlinear EH model as well as complicated Q-function in FBL model, the formulated joint resource allocation problem is non-convex and cannot be efficiently solved by convex optimization tools. To address the original problem (OP), we first decoupled the supply and consumption relationship between WPT and WIT phase and decomposed OP into two sub-problems (i.e., power allocation problem and blocklength allocation problem). Although the sub-problems are relatively more tractable due to lower dimensionality of optimization variables, they are still non-convex. To cope with it, we transferred the original nonconvex power allocation subproblem into multiple convex local problems through slack variables introduction, variable substitution and SCA algorithm. In blocklength allocation problem, we converted the nonconvex constraint into a convex one through SCA algorithm and proved the convexity of FBL error probability with respect to WIT blockength. Finally, a suboptimal solution of the original problem can be obtained by alternatingly addressing the subproblems. Via simulation, we validated the accuracy and efficiency of our proposed alternating-based algorithm and investigated the performance advantage of our joint resource allocation design. Based on the numerical results, a set of guidelines are also provided for practical system design.

REFERENCES

[1] S. Verma, S. Kaur, M. A. Khan, and P. S. Sehdev, "Toward green communication in 6G-enabled massive Internet of Things," *IEEE Internet Things J.*, vol. 8, no. 7, pp. 5408–5415, Apr. 2021.

[2] O. Cetinkaya, E. Dinc, C. Koca, G. V. Merrett, and O. B. Akan, "Energy-neutral wireless-powered networks," *IEEE Wireless Commun. Lett.*, vol. 8, no. 5, pp. 1373–1376, Oct. 2019.

[3] Y. He, S. Zhang, L. Tang, and Y. Ren, "Large scale resource allocation for the Internet of Things network based on ADMM," *IEEE Access*, vol. 8, pp. 57192–57203, 2020.

[4] T. Wang, X. Yang, F. Deng, L. Gao, Y. Jiang, and Z. Yang, "Joint power and duty-cycle design using alternating optimization algorithm under energy harvesting architectures," *China Commun.*, vol. 17, no. 12, pp. 139–155, Dec. 2020.

[5] P. Chen, X. Zhou, J. Zhao, F. Shen, and S. Sun, "Energy-efficient resource allocation for secure D2D communications underlaying UAV-enabled networks," *IEEE Trans. Veh. Technol.*, vol. 71, no. 7, pp. 7519–7531, Jul. 2022.

[6] J. Chen, Z. Zhang, Y.-C. Liang, X. Kang, and R. Zhang, "Resource allocation for wireless-powered IoT networks with short packet communication," *IEEE Trans. Wireless Commun.*, vol. 18, no. 2, pp. 1447–1461, Feb. 2019.

[7] R. Ma, H. Wu, J. Ou, S. Yang, and Y. Gao, "Power splitting-based SWIPT systems with full-duplex jamming," *IEEE Trans. Veh. Technol.*, vol. 69, no. 9, pp. 9822–9836, Sep. 2020.

[8] F. Deng, X. Yue, X. Fan, S. Guan, Y. Xu, and J. Chen, "Multisource energy harvesting system for a wireless sensor network node in the field environment," *IEEE Internet Things J.*, vol. 6, no. 1, pp. 918–927, Feb. 2019.

[9] G. Kwon, H. Park, and M. Win, "Joint beamforming and power splitting for wideband millimeter wave SWIPT systems," *IEEE J. Sel. Topics Signal Process.*, vol. 15, no. 5, pp. 1211–1227, Aug. 2021.

[10] Z. Zou, A. Gidmark, T. Charalambous, and M. Johansson, "Optimal radio frequency energy harvesting with limited energy arrival knowledge," *IEEE J. Sel. Areas Commun.*, vol. 34, no. 12, pp. 3528–3539, Dec. 2016.

[11] Y. Xiao, D. Niyato, Z. Han, and L. A. DaSilva, "Dynamic energy trading for energy harvesting communication networks: A stochastic energy trading game," *IEEE J. Sel. Areas Commun.*, vol. 33, no. 12, pp. 2718–2734, Dec. 2015.

[12] C. In, H.-M. Kim, and W. Choi, "Achievable rate-energy region in two-way decode-and-forward energy harvesting relay systems," *IEEE Trans. Commun.*, vol. 67, no. 6, pp. 3923–3935, Jun. 2019.

[13] D. Altinel and G. K. Kurt, "Modeling of multiple energy sources for hybrid energy harvesting IoT systems," *IEEE Internet Things J.*, vol. 6, no. 6, pp. 10846–10854, Dec. 2019.

[14] P. Nezhadmohammad, M. Abedi, M. J. Emadi, and R. Wichman, "SWIPT-enabled multiple access channel: Effects of decoding cost and non-linear EH model," *IEEE Trans. Commun.*, vol. 70, no. 1, pp. 306–316, Jan. 2022.

[15] S. Jang, H. Lee, S. Kang, T. Oh, and I. Lee, "Energy efficient SWIPT systems in multi-cell MISO networks," *IEEE Trans. Wireless Commun.*, vol. 17, no. 12, pp. 8180–8194, Dec. 2018.

[16] F. Wang, J. Xu, and S. Cui, "Optimal energy allocation and task offloading policy for wireless powered mobile edge computing systems," *IEEE Trans. Wireless Commun.*, vol. 19, no. 4, pp. 2443–2459, Apr. 2020.

[17] Y. Du, K. Yang, K. Wang, G. Zhang, Y. Zhao, and D. Chen, "Joint resources and workflow scheduling in UAV-enabled wirelessly-powered MEC for IoT systems," *IEEE Trans. Veh. Technol.*, vol. 68, no. 10, pp. 10187–10200, Dec. 2019.

[18] P. Zhao, W. Zhao, H. Bao, and B. Li, "Security energy efficiency maximization for untrusted relay assisted NOMA-MEC network with WPT," *IEEE Access*, vol. 8, pp. 147387–147398, 2020.

[19] A. Khazali, D. Tarchi, M. G. Shayesteh, H. Kalbkhani, and A. Bozorgchenani, "Energy efficient uplink transmission in cooperative mmWave NOMA networks with wireless power transfer," *IEEE Trans. Veh. Technol.*, vol. 71, no. 1, pp. 391–405, Jan. 2022.

[20] C. Wu, X. Mu, Y. Liu, X. Gu, and X. Wang, "Resource allocation in STAR-RIS-Aided networks: OMA and NOMA," *IEEE Trans. Wireless Commun.*, vol. 21, no. 9, pp. 7653–7667, Sep. 2022, doi: 10.1109/TWC.2022.3160151.

[21] L. Sun, L. Wan, K. Liu, and X. Wang, "Cooperative-evolution-based WPT resource allocation for large-scale cognitive industrial IoT," *IEEE Trans. Ind. Informat.*, vol. 16, no. 8, pp. 5401–5411, Aug. 2020.

[22] Z. Chang, L. Lei, H. Zhang, T. Ristaniemi, S. Chatzinotas, B. Ottersten, and Z. Han, "Energy-efficient and secure resource allocation for multiple-antenna NOMA with wireless power transfer," *IEEE Trans. Green Commun. Netw.*, vol. 2, no. 4, pp. 1059–1071, Dec. 2018.

[23] X. Kang, C. K. Ho, and S. Sun, "Optimal time allocation for dynamic-TDMA-based wireless powered communication networks," in *Proc. IEEE Global Commun. Conf.*, Austin, TX, USA, Dec. 2014, pp. 3157–3161.

[24] Z. Yang, Y. Pan, C. Pan, and M. Chen, "Optimal fairness-aware time and power allocation in wireless powered communication networks," *IEEE Trans. Commun.*, vol. 66, no. 7, pp. 3122–3135, Jul. 2018.

[25] D. Mishra and S. De, "Optimal time allocation for RF-powered DF relay-assisted cooperative communication," *Electron. Lett.*, vol. 52, no. 14, pp. 1274–1276, Jul. 2016.

[26] J. Feng, W. Zhang, Q. Pei, J. Wu, and X. Lin, "Heterogeneous computation and resource allocation for wireless powered federated edge learning systems," *IEEE Trans. Commun.*, vol. 70, no. 5, pp. 3220–3233, May 2022.

[27] Z. Chang, Z. Wang, X. Guo, C. Yang, Z. Han, and T. Ristaniemi, "Distributed resource allocation for energy efficiency in OFDMA multicell networks with wireless power transfer," *IEEE J. Sel. Areas Commun.*, vol. 37, no. 2, pp. 345–356, Feb. 2019.

[28] Y. Hu, X. Yuan, T. Yang, B. Clerckx, and A. Schmeink, "On the convex properties of wireless power transfer with nonlinear energy harvesting," *IEEE Trans. Veh. Technol.*, vol. 69, no. 5, pp. 5672–5676, May 2020.

[29] Z. Wei, S. Sun, X. Zhu, D. In Kim, and D. W. K. Ng, "Resource allocation for wireless-powered full-duplex relaying systems with nonlinear energy harvesting efficiency," *IEEE Trans. Veh. Technol.*, vol. 68, no. 12, pp. 12079–12093, Dec. 2019.

[30] N. Guo, X. Yuan, Y. Hu, and A. Schmeink, "SWIPT-enabled multi-user cooperative communication with nonlinear energy harvesting," in *Proc. 25th Int. ITG Workshop Smart Antennas*, French Riviera, France, Nov. 2021, pp. 1–6.

[31] Y. Lu, K. Xiong, P. Fan, Z. Ding, Z. Zhong, and K. Letaief, "Global energy efficiency in secure MISO SWIPT systems with non-linear power-splitting EH model," *IEEE J. Sel. Areas Commun.*, vol. 37, no. 1, pp. 216–232, Jan. 2019.

[32] R. Jiang, K. Xiong, P. Fan, Y. Zhang, and Z. Zhong, "Power minimization in SWIPT networks with coexisting power-splitting and time-switching users under nonlinear EH model," *IEEE Internet Things J.*, vol. 6, no. 5, pp. 8853–8869, Oct. 2019.

[33] J.-M. Kang, I.-M. Kim, and D. I. Kim, "Joint Tx power allocation and Rx power splitting for SWIPT system with multiple nonlinear energy harvesting circuits," *IEEE Wireless Commun. Lett.*, vol. 8, no. 1, pp. 53–56, Feb. 2019.
[34] A. M. Obais and A. F. Ruzij, "Design and implementation of an efficient WPT system," *Int. J. Electr. Power Energy Syst.*, vol. 11, pp. 711–725, Jun. 2020.
[35] A. Sarin and A.-T. Avestruz, "A framework for code division multiple access wireless power transfer," *IEEE Access*, vol. 9, pp. 135079–135101, 2021.
[36] X. Yuan, Y. Hu, R. Schober, and A. Schmeink, "Convexity analysis of nonlinear wireless power transfer with multiple RF sources," *IEEE Trans. Veh. Technol.*, vol. 71, no. 10, pp. 11311–11316, Oct. 2022.
[37] R. Hamdi, M. Chen, A. B. Said, M. Qaraqe, and H. V. Poor, "Federated learning over energy harvesting wireless networks," *IEEE Internet Things J.*, vol. 9, no. 1, pp. 92–103, Jan. 2022.
[38] N. Guo, X. Yuan, Y. Hu, F. Chong, and A. Schmeink, "Reliability-oriented resource allocation for multi-source WPT enabled multi-user short packet communications," in *Proc. IEEE ISWCS*, Hangzhou, China, Oct. 2022, pp. 1–6.
[39] N. Guo, X. Yuan, Y. Hu, and A. Schmeink, "Wireless powered short packet communications with multiple WPT sources," 2023, *arXiv:2302.12396*.
[40] C. She, C. Yang, and T. Q. S. Quek, "Cross-layer optimization for ultra-reliable and low-latency radio access networks," *IEEE Trans. Wireless Commun.*, vol. 17, no. 1, pp. 127–141, Jan. 2018.
[41] Y. Polyanskiy, H. V. Poor, and S. Verdu, "Channel coding rate in the finite blocklength regime," *IEEE Trans. Inf. Theory*, vol. 56, no. 5, pp. 2307–2359, Apr. 2010.
[42] Y. Hu, Y. Zhu, M. C. Gursoy, and A. Schmeink, "SWIPT-enabled relaying in IoT networks operating with finite blocklength codes," *IEEE J. Sel. Areas Commun.*, vol. 37, no. 1, pp. 74–88, Jan. 2019.

NING GUO (Student Member, IEEE) is currently pursuing the M.E. degree with Wuhan University, Wuhan, China. Her research interests include ultra-reliable low-latency communication, wireless power transfer networks, and optimization technology.

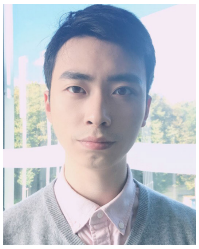

XIAOPENG YUAN (Graduate Student Member, IEEE) received the B.Sc. degree in automation from the Beijing University of Aeronautics and Astronautics, China, in 2016, and the M.Sc. degree in electrical engineering, information technology and computer engineering from RWTH Aachen University, Germany, in 2019, where he is currently pursuing the Ph.D. degree. His research interests include UAV-assisted wireless networks, wireless power transfer networks, ultra-reliable low-latency communication networks, trajectory design, and optimization technology.

YULIN HU (Senior Member, IEEE) received the M.Sc.E.E. degree from USTC, China, in 2011, and the Ph.D.E.E. degree (Hons.) from RWTH Aachen University. He successfully defended his dissertation of a joint Ph.D. Program supervised by Prof. Anke Schmeink with RWTH Aachen University and Prof. James Gross with the KTH Royal Institute of Technology, in December 2015. He was a Postdoctoral Research Fellow with RWTH Aachen University, from January 2016 to December 2016. He was a Senior Researcher and the Team Leader with Prof. Anke Schmeink with ISEK Research Area, RWTH Aachen University. From May 2017 to July 2017, he was a Visiting Scholar with Prof. M. Cenk Gursoy with Syracuse University, USA. He is currently a Professor with the School of Electronic Information, Wuhan University, and an Adjunct Professor with ISEK Research Area, RWTH Aachen University. His research interests include information theory and the optimal design of wireless communication systems. He served as a TPC member for many conferences. He has been invited to contribute submissions to multiple conferences. He was a recipient of the IFIP/IEEE Wireless Days Student Travel Awards, in 2012. He received the Best Paper Awards at IEEE ISWCS 2017 and IEEE PIMRC 2017. He was the Lead Editor of the Urllc-LoPIoT Special Problem in Physical Communication and an Organizer and the Chair of two special sessions at IEEE ISWCS 2018 and ISWCS 2021. He is serving as the Editor for IEEE TRANSACTIONS ON VEHICULAR TECHNOLOGY, *Physical Communication* (Elsevier), *EURASIP Journal on Wireless Communications and Networking*, and *Frontiers in Communications and Networks*.

ANKE SCHMEINK (Senior Member, IEEE) received the Diploma degree in mathematics with a minor in medicine and the Ph.D. degree in electrical engineering and information technology from RWTH Aachen University, Germany, in 2002 and 2006, respectively. She was a Research Scientist with Philips Research, before joining RWTH Aachen University, in 2008. Since 2012, she has been a Professor with RWTH Aachen University. She has spent several research visits with The University of Melbourne and the University of York. Her research interests include information theory, machine learning, data analytics, and optimization with a focus on wireless communications and medical applications. She is a member of the Young Academy with the North Rhine-Westphalia Academy of Sciences.